Urban Climate 45 (2022) 101284

Contents lists available at ScienceDirect

Urban Climate

journal homepage: www.elsevier.com/locate/uclim

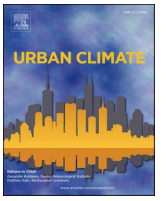

Using Machine Learning to estimate the impact of different modes of transport and traffic restriction strategies on urban air quality

Alexandre Fabregat, Anton Vernet *, Marc Vernet, Lluís Vázquez, Josep A. Ferré

Department of Mechanical Engineering, Universitat Rovira i Virgili, Av. Päsos Catalans 26, 43007 Tarragona, Spain

ARTICLE INFO

Keywords:
Machine Learning
Low Emission Zone
Urban pollution
COVID-19
Pollutant dispersion
Air quality
Transportation emissions

ABSTRACT

Classical pollutant dispersion models, based on the numerical resolution of some approximate form of the momentum, energy and chemical species conservation equations, are usually limited by incomplete descriptions of the atmospheric boundary layer hydrodynamics, partial characterizations of the emission inventories and, often, high computational costs. Using the metropolitan area of Barcelona as benchmark, the Machine Learning aproach presented here alleviates these limitations providing very accurate local predictions of key pollutant concentrations. Originating mostly from Open Data sources, time-series data on road, maritime and air traffic along with meteorological records from October 2017 to June 2021, have allowed, by means of Machine Learning techniques, to create a model capable of estimating the individual contributions of each mode of transport to worsened Air Quality. Also, when used to investigate the impact of recently implemented mitigation measures, model results predict a reduction of approximately 8 $\mu g \cdot m^{-3}$ for CO and NO_x. In contrast, O_3, PM_{10} and SO_2 are found to be unaffected. The COVID-19 lockdown provided an accidental opportunity to improve the model's robustness and predictive capability through unusually low emission rates from transportation.

1. Introduction

Urban air pollution, mostly originated from combustion sources, has been shown to harm humans causing a wide spectrum of health effects ranging from eye irritation to death (Cohen et al., 2006; Maynard, 2009; Liang and Gong, 2020; B, 2010; Cohen et al., 2017). Globally, fossil fuel-based transort is estimated to be responsible for more than 50% of the NO_x emissions, of which road traffic, shipping and aviation account for 51%, 27% and 11% respectively (European Environment Agency, 2021). Despite the gradual implementation of environmental policies and measures aimed at reducing their impact, airborne pollutants are still behind a significant number of premature deaths even in the locations with the most restrictive regulations (Khomenko et al., 2021). Despite differences in Air Quality standards between different countries and regions, the local concentration of key pollutants in the urban canopy is a central metric in evaluating how healthy is the air we breath (World Health Organization, 2021).

In this context, understanding the physical and chemical processes responsible for the transport and dispersion of pollutants is crucial to assess the effectiveness of any action aimed at improving the air quality by, for example, restricting traffic in central city districts or providing incentives for the electrification of the automobile fleet. Predicting the local pollutant concentration in urban areas is, however, challenging due to the relatively wide range of spatial and temporal scales over which transport may occur. Thus, a

* Corresponding author.
E-mail addresses: alexandre.fabregat@urv.cat (A. Fabregat), anton.vernet@urv.cat (A. Vernet), mrcvs31@gmail.com (M. Vernet), lluis.vazquez@urv.cat (L. Vázquez), josep.a.ferre@urv.cat (J.A. Ferré).

https://doi.org/10.1016/j.uclim.2022.101284
Received 27 March 2022; Received in revised form 5 August 2022; Accepted 1 September 2022
Available online 15 September 2022

mechanistic model for pollutant dispersion in urban environments has to take into account the local turbulent hydrodynamics of the atmosphere which, in turn, will depend on the urban ground topology and the surface heat budget among others. In addition, this model will also need a detailed pollutant inventory and emission rates of the different relevant chemical species from all sort of sources including the mobile ones and the chemical transformation and deposition they may undergo (Li et al., 2021; Lateb et al., 2016; Sachdeva and Baksi, 2018).

From the physics point of view, the transport of a chemical species i, e.g., an airborne pollutant, is governed by the convection-diffusion-reaction equation,

$$\frac{\partial \rho Y_i}{\partial t} + \nabla \cdot (\rho \overrightarrow{u} Y_i) = -\nabla \overrightarrow{J_i} + R_i + S_i \tag{1}$$

where ρ is the density of the fluid mixture, t is time, $\overrightarrow{u}$ is the velocity field of the fluid mixture, Y_i is the mass fraction of chemical species i, R_i accounts for any generation/consumption of i due to chemical reaction and S_i represents any other source/sink of i. In most air pollution applications, the fluid is assumed incompressible and S_i is used to account for pollutant source emissions, surface deposition and any physicochemical processes other than reaction. Given the highly turbulent nature of the atmospheric air currents, the convective contribution to the overall transport of i is usually many orders of magnitude larger than that due to diffusive effects.

Exact solutions of Eq. (1) are often infeasible due to the impossibility of accessing (1) the turbulent field of instantaneous velocity $\overrightarrow{u}(\overrightarrow{x}, t)$ and (2) the precise inventory of pollutant emissions accounted for in the S_i term.

Different strategies to obtain approximate solutions to Eq. (1) have been developed over the years. For instance, Gaussian Dispersion Models provide time-averaged concentration fields by assuming constant wind velocity and direction and parametrizing the turbulent transport contribution (Gifford, 1976; Pasquill, 1976). As computational capabilities increased, modern approaches relied on the numerical solution of Partial Differential Equations (PDEs) that usually involve the spatial and temporal discretization of Eq. (1). In this context, the use of progressively finer grids that concentrate the resolution over the region of interest, data assimilation methodologies and other specific developments have enabled to address the complex multiscale nature of the problem of pollutant dispersion in urban areas and improve predictive capabilities (see for instance (Beevers et al., 2013; Munir et al., 2020)). State-of-the-art operational mesoscale air quality forecast systems often combine specific modules for meteorology, atmospheric chemistry, urban topology and pollutant emissions inventory to bridge the various physical aspects that govern the airborne transport of hazardous species. For instance, CALIOPE-Urban (Benavides et al., 2019), used to investigate pollutant dispersion in the city of Barcelona, integrates several packages including HERMES for emission inventory (Guevara et al., 2013; Guevara et al., 2019), the WRF numerical weather prediction system (Skamarock and Klemp, 2006; Powers et al., 2017) and CMAQ Multiscale Air Quality Modeling System (Byun and Schere, 2006; Eder and Yu, 2006) coupled with the urban roadway dispersion model R-LINE (Snyder et al., 2013).

This and the vast majority of other physics-based models that rely on solving the transport equations are, however, often limited by (1) the lack of accurate pollutant inventories and (2) potentially large computational resources. In a context of rapid penetration of Machine Learning (ML) and Artificial Intelligence (AI) techniques in practically all areas of knowledge, their use in pollutant dispersion applications has demonstrated their ability to alleviate these limitations. On the one hand, these tools can exploit pollutant concentration and meteorology data sets that are usually publicly available, albeit with varying degrees of spatial and temporal resolution. On the other hand, although model training can be computationally intensive, their cost for prediction purposes is usually significantly cheaper than that associated with solving PDEs (Li et al., 2020a; Lu et al., 2021). In the recent years, ML and AI have been used in the development of Air Quality predictive tools for densely populated areas (Lu and Wang, 2005; Russo et al., 2013; Garcia Nieto et al., 2013; Singh et al., 2013), investigate the impact of Air Pollution on the incidence of respiratory diseases (Polezer et al., 2018) and assess the effects of COVID-19 lockdown on local pollutant levels (Rybarczyk and Zalakeviciute, 2021; Guevara et al., 2021). Since then, the use of these techniques to improve our understanding of urban air pollution has not ceased (Masih, 2019; Gómez et al., 2020). For an updated although not exhaustive list of previous works see Kumar and Pande (Kumar and Pande, 2022).

Among the type of learners, Support Vector Regression (SVR) and Long Short-Term Memory (LSTM) methods have been widely used to predict different Air Quality metrics using historical data from relatively long time series (Kumar and Pande, 2022; Yang et al., 2018; Ma et al., 2019; Liu et al., 2017; Dun et al., 2020; Castelli et al., 2020; Chau et al., 2022). For instance, Castelli et al. (Castelli et al., 2020) used ML techniques to forecast concentration levels of selected pollutants and Air Quality Index (AQI) in California using time-series statistics (roll mean and lag) along with meteorological data.

Previous works can also be categorized based on the type of predicted response. Thus, models can either be used to predict pollutant concentration levels (regression) (Chau et al., 2022; Fabregat et al., 2021) or classify the AQI into a given category (classification) (Castelli et al., 2020; Kleine Deters et al., 2017).

Differences between models stem also from the number and type of predictors. In some cases the response is predicted using only previous values from time series of, for instance, pollutant concentration recorded by measuring stations (Dun et al., 2020; Zalakeviciute et al., 2020). On the other hand, models may use meteorology and other predictors to elucidate the dependency of the response upon them (Chau et al., 2022; Kleine Deters et al., 2017; Simic et al., 2020). As an example, Šimić et al. (Simic et al., 2020) combined meteorological features and daily pollutant concentration samples in the center of Zagreb (Croatia) over the time span of three years to assess the capacity of several ML learners to predict the daily concentration of PM10, NO2, elementary and organic carbon. Additional predictors have been included to better capture the response variability due to mobility patterns. For example, Arnaudo et al. (Arnaudo et al., 2020) included traffic data derived from the passage of vehicles recorded from fixed video cameras in a belt surrounding the city of Milan.

The COVID-19 pandemic lockdown responsible for a significant reduction of mobility and therefore transportation emissions have

been identified as an opportunity to improve the model robustness by training the models with unusually low traffic intensities. For example, Lovric et al. (Lovric et al., 2021) used ML techniques to estimate the impact of COVID-19 lockdown on the air pollution levels in Graz (Austria) by considering the road traffic intensity as a feature along with meteorological data. Other efforts directed at improving the predictor quality were aimed at increasing the spatial resolution of concentration records by means of mobile pollutant measuring stations (Song et al., 2021; Zhao et al., 2021).

Fabregat et al. (Fabregat et al., 2021) used Machine Learning techniques to build a model capable of accurately predicting the local pollutant levels in the metropolitan area of Barcelona using historical data on meteorology and traffic intensity between October 2017 to March 2020. The predictive capability of the model, used to estimate the impact associated with cruise ship activity in the city Port, suggested that Machine Learning approaches are a viable alternative to physics-based models and allow to estimate the individual impact of different predictors on air quality using public and readily available data with very modest computational resources.

Using again the city of Barcelona as benchmark, the goal of the present work is to improve the original model developed by Fabregat et al. *(*Fabregat et al., 2021*)* and use it to (i) estimate the individual contributions of each transportation mode (road, air and maritime) to increased pollutant concentration and (ii) to assess the effectiveness of recently implemented mitigation measures (Low Emission Zone or LEZ) aimed at improving the Air Quality in Barcelona (Benavides et al., 2020; Departament d'Avaluació i Gestió Ambiental, 2022).

In comparison to the analysis in Fabregat et al. *(*Fabregat et al., 2021*)*, the predictor set in the present work has been extended with additional variables that may potentially contribute to better explain the pollutant concentration variability. First, we included a background PM_{10} concentration feature that is expected to capture non-local contributions to the particulate matter levels due to wildfires and/or Saharan dust episodes that are not associated with local transportation emissions. Second, we added a categorical feature that allows to distinguish when the Low Emission Zone that restricts the most pollutant vehicles access to the metropolitan area are in effect (Grup d'Avaluació de l'Impacte de la Zona de Baixes Emissions ZBE Rondes Barcelona, 2021). In addition, the set of observations, covering the interval from October 2017 to June 2021, now includes the COVID-19 lockdown period. Although studying the effect of COVID-19 on air pollution is not one of the objectives of this work, the existence of a low activity period provides an unexpected opportunity to extend the training domain with exceptionally low levels of traffic intensity and industrial production (Dutheil et al., 2020; Kerimray et al., 2020; Li et al., 2020b).

The approach presented here differs from previous works in two main key points. First, given the potential role played by Airports and Ports on the local Air Quality of neighboring cities (Degraeuwe et al., 2019a), here we used feature engineering to consider dedicated predictors aimed at capturing the impact of these two transportation modes along with road traffic. Second, the methodology presented here is not intended to provide a forecast of the concentration but to estimate the impact of each transportation mode and, more importantly, the effectiveness of air pollution mitigation measures at several locations across the metropolitan area of Barcelona. While notable success in forecasting the pollutant concentration using historical data has been already demonstrated, estimations of the individual share for each pollutant source and road traffic restrictions has not been as thoroughly explored. In this work we demonstrate that it is possible to accurately quantify individual contributions to increased pollutant concentrations in urban environments without detailed atmospheric hydrodynamics or precise source inventories.

This present manuscript is organized as follows: Setion 2 describes the methods and materials used to build the working dataset as well as the model development methodology. Section 3 presents the main results and quantifies the contribution of each transportation mode to increased pollutant concentration for several chemical species and locations across the metropolitan area. The effectiveness of traffic restrictions imposed in the city of Barcelona to improve air quality in the metropolitan area is also evaluated. Section 4 discusses the hypothesis, assumptions and potential future improvements to the current methodology and Section 5 summarizes the major findings.

Table 1
List of predictors, their description and the number of levels for those that have been One-Hot-Encoded (OHE). If used, normalization by subtracting the mean and dividing by the standard deviation is indicated.

j	Predictor	Description	OHE levels	Normalized
1	wind vel	Wind velocity	–	✓
2	temp	Temperature	–	✓
3	hum rel	Relative humidity	–	✓
4	press	Atmospheric pressure	–	✓
5	precipita	Precipitation	–	✓
6	insol	Solar irradiance	–	✓
7	wind dirx	East-West wind component	–	–
8	wind diry	North-South wind component	–	–
9	alig port	Port-station alignment	–	–
10	alig aero	Airport-station alignment	–	–
11	port numv	Number of docked vessels	–	✓
12	aero numf	Number of flight operations	–	✓
13	backPM10	Background PM_{10} concentration	–	✓
14	density	Road traffic density	–	✓
15	LEZ	Low Emission Zone	2	–
16	hday	Hour of the day	24	–
17	month	Month of the year	12	–
18	code	Pollution measurement station ID	7	–

2. Materials and methods

In the context of ML/AI, the present application is of the *Supervised Learning* type. The objective is to elucidate, if it exists, the dependence f between a *response* and a set of *predictors* on which it depends using large sets of observations from which f can be 'learned'. Here, the response is the hourly value of concentration of a given pollutant c_i. The set of predictors (or features) $\boldsymbol{x}_j = (x_1, x_2, \ldots, x_n)$ is comprised of $j = 1 \ldots n$ variables that, in accordance with the physics governing the dispersion of pollutants in the air, are expected to affect the response and include the instantaneous local weather and atmospheric conditions and the emissions inventory. The goal is to find a good approximation of f, namely $\widehat{f}$, to obtain accurate predictions of c_i using $\widehat{c} = \widehat{f}(x_j)$ and use it to determine the individual impact of a given predictor on the pollutant concentration, this is, estimating the first-order effects of the form $\partial c_i/\partial x_j$.

2.1. Working dataset

The working dataset is comprised of hourly synchronous observations of pollutant concentration (the response) and the $n = 18$ different predictors shown in Table 1. This table lists the features that, for convenience or due to its categorical nature, have been one-hot-encoded for appropriate use in the model training indicating the number of levels. Also, following the standard procedure, the continuous predictors that have been normalized by subtracting the mean and dividing by the standard deviation are also identified.

In total, the working dataset consists of 23,427 hourly observations amounting to a 72.5% completeness with respect to the theoretical 32,300 observations covering the sampling time period from 2017 to 10-01 to 2021-06-07. While most missing observations are randomly scattered in time, a temporary interruption in the road traffic data gathering during the COVID-19 lockdown produced a continuous gap of 1932 h. Given the relevance of the data interruption both in terms of size and timing (at the very beginning of the pandemic lockdown), traffic density over the missing time span have been estimated using ML techniques. Details on the methodology can be found in Appendix A. Following a conservative approach, only those hourly observations for which concentration data exist for all measurement stations have been considered. Thus, the total number of rows in the working data set is about half a million.

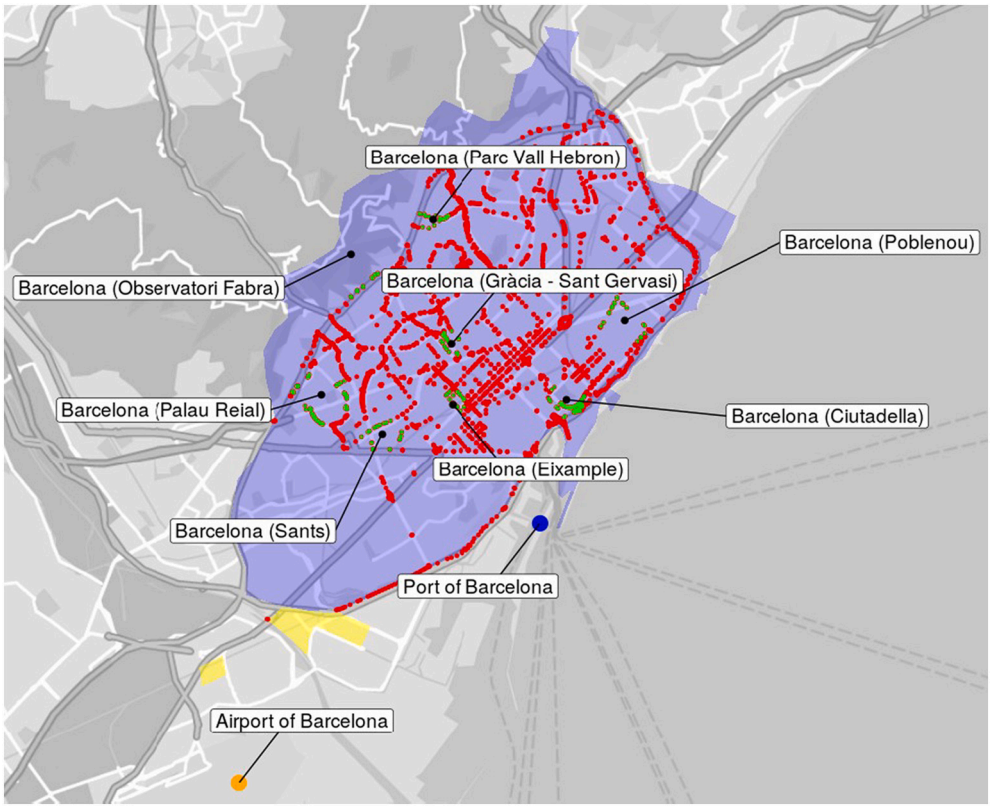

Fig. 1. Map of the Barcelona metropolitan area showing the location and names of the pollutant stations (black markers), the Port (blue marker) and the Airport (orange marker). Traffic density measurement locations are shown as red and green markers where the latest have been used to estimate the local value in the vicinity of each pollutant station. The area enclosed by the Low Emission Zone is depicted using a blue overlay. Yellow areas show the location of the two major industrial sites. (For interpretation of the references to colour in this figure legend, the reader is referred to the web version of this article.)

2.1.1. Pollutant concentration

The hourly data on pollutant concentration in $\mu g/m^3$ for m = 7 different pollutant species has been obtained from $p = 7$ measurement station across the metropolitan area of Barcelona belonging to the Air Pollution Monitoring and Forecasting Network (XVPCA) of the Department of Climate Action, Food and Rural Agenda of the Generalitat de Catalunya (Medi ambient i sostenibilitat, 2022). The pollutant species are carbon monoxide CO, nitric oxide NO, nitrogen dioxide NO_2, total nitrogen oxides NO_x, ozone O_3, suspended particulate matter of 10 μm of diameter or less PM_{10} and sulfur dioxide SO_2. The location of the pollutant measurement stations is shown in Fig. 1 as black markers (names of the stations are also indicated). Although Fig. 1 shows 8 pollutant measurement stations, the one named *Observatory Fabra* has been discarded, first, because unlike the rest of the stations of the *Urban Background* or *Urban Traffic* types, this one belongs to the *Background Suburban* type. Secondly, as shown in Fig. 1, it is the only one located outside the limits of the metropolitan area where no nearby traffic data exists. Finally, this station height with respect to the sea level (415 m) departs significantly from the rest of stations which altitude ranges between from 3 to 136 m. It is worth noting that not all $p = 7$ stations measure all m = 7 pollutants. The list of stations, their type and data availability for each pollutant species is shown in Appendix B.

Although the PM10 concentration, as well as all other pollutants, is the response in the present ML application, its far-field background value is used here as a predictor to account for contributions to particulate matter levels not attributable to local emissions but due to, for instance, intense Saharan dust episodes or forest fires. Using the same pollutant measurement station network all concentration data has been retrieved from (Medi ambient i sostenibilitat, 2022), the PM10 concentration at a rural station has been used here as a predictor for background particulate matter levels. The location of this station, near the town of Sort (42°24′36" N — 1°07′43″ E) and approximately 140 km from the Barcelona metropolitan area, is shown in Appendix C.

2.1.2. Meteorology

The meteorological data (wind direction and velocity, temperature, relative humidity, precipitation, atmospheric pressure and irradiance) is available with a 30-min sampling rate obtained from two measurement stations belonging to the Network of Automatic Weather Stations of the Catalan Meteorologic Service (XEMA) (Servei Meteorològic de Catalunya (Catalan Meteorologic Service), 2022). Given the high levels of correlation in the meteorological predictors between these two stations within the metropolitan area of Barcelona located roughly 6 km from each other (see the map in Appendix D), the average between these two stations have been used as a representative state of the local atmosphere across the metropolitan area. Each pair of consecutive 30 min data points have also been averaged to obtain a single value per hour to enable the dataset merging with the rest of predictors with a nominal hourly sampling rate. The temporal evolution of meteorologic predictors over 2020 is shown in Appendix E.

2.1.3. Road traffic

The road traffic density data has been retrieved from the traffic state network of the city of Barcelona Open Data portal (Open Data BCN, 2022a). The measurement locations are shown in Fig. 1 as red and green markers. Importantly, data comes as a normalized number of vehicles per meter of traffic route taking integer values between 1 (fluid traffic) and 5 (congested traffic). For each pollutant measurement station, the value of the traffic density has been estimated by taking the average of the traffic density over the closest locations (marked in green in Fig. 1). In this work we assume that this variable works as a proxy of the road traffic emission intensity.

Road traffic data stream was interrupted at the beginning of the COVID19 pandemic lockdown in March 2020. The resulting gap has been imputated using alternative data on mobility in the city of Barcelona as explained in Appendix A.

2.1.4. Air traffic

Hourly total number of flights to and from the Airport of Barcelona have been provided on request by the European Organisation for the Safety of Air Navigation, commonly known as Eurocontrol (Nicolas, 2022). The map in Fig. 1 shows the location of the Airport of Barcelona as an orange dot. The number of movements at the Airport of Barcelona between February 2020 and April 2020 illustrating the impact of the COVID-19 lockdown on mobility is shown in Appendix F.

In this work it is assumed that the total emissions of the Airport of Barcelona are highly correlated with the number of flight movements in this infrastructure and therefore the impact of the Airport can be adequately characterized by this predictor.

2.1.5. Maritime traffic

Hourly number of both total vessels and cruise ships docked at the Port of Barcelona have been retrieved from its Open Data portal (Port of Barcelona Open Data Portal, 2022). The map in Fig. 1 shows the location of the Port of Barcelona as a blue dot. The number of hourly total vessels docked at the Port of Barcelona between January 2019 and December 2020, the percentage of those vessels that are cruise liners and the length of stays distribution are shown in Appendix G.

As it happened for the number of flight movements, here it is assumed that the total emissions of the Port of Barcelona are highly correlated with the number of docked vessels and therefore the impact of the Port can be properly accounted by this predictor.

2.1.6. Other predictors

The local government of Barcelona imposed a Low Emission Zone or LEZ (*Zona de Baixes Emissions* or ZBE in Catalan) to limit access to the metropolitan area of the city and reduce pollution levels in the city. Although effective from January 1, 2020, a moratorium postponed the start of sanctions until September 15, 2020. The measures restrict the entry of those vehicles identified as the most polluting according to their year of purchase and engine type. Details of the vehicles affected by this restriction are provided in Appendix H. To account for the impact associated with the Low Emission Zone, we defined a categorical predictor that takes the value

of 1 after September 15, 2020 and 0 otherwise. With an extension of 95 km^2, the LEZ is shown in Fig. 1 as a blue overlay.

For reference and due to their potential role in contributing to pollutant emissions, the two major industrial sites between the metropolitan area and the Airport of Barcelona are shown in Fig. 1 as yellow overlays.

2.2. Pre-processing and data preparation

Code for data cleaning, pre-processing and feature engineering was written in R version 3.6.3. Code for model training, resampling, hyperparameter tuning and post-processing was written in python 3.7.

Following standard procedures, the relatively large values of skewness in the pollutant concentration, wind velocities and background PM_{10} distributions was alleviated using a logarithmic transformation.

Regarding feature engineering, wind direction reported by the direction from which it originates expressed as angle in degrees in a cardinal points was transformed into a set of four predictors. Two of them were the cosine and the sine of the wind direction angle (*wind dirx* and *wind diry*). The other two were the wind alignment between each measuring station and the Port and the Airport of Barcelona (see Fig. 1). Alignment with respect to the Port and the Airport of Barcelona was computed respectively as

$$a_P = \left(1 - \frac{|\beta - \gamma_P|}{180}\right)^2 \tag{2}$$

$$a_A = \left(1 - \frac{|\beta - \gamma_A|}{180}\right)^2 \tag{3}$$

where β is the wind direction angle and γ_P and γ_A are the angles of the lines connecting each pollutant measurement station and the Port or the Airport respectively. Both alignment values are bounded in the [0,1] interval where 0 indicates wind blowing in the opposite direction to the line connecting the station and the corresponding infrastructure while 1 indicates perfect alignment. Importantly, while the meteorological data is shared by all pollutant measurement stations, each of them has been trained with their corresponding data on road traffic density and port and airport alignment.

All predictors in the form of time series have been smoothed using a triangular and symmetrical 7-h window to (i) remove the highest frequency fluctuations in the signal associated to the finest scales in the environmental turbulence and (ii) reduce the number of degrees of freedom in the learner and the CPU time during the model training. The 7-h window with relative weights (1/4, 2/4, 3/4, 1, 3/4, 2/4, 1/4) must not to be understood as an optimized parameter but as an heuristic criteria related to daily periodic behaviour of the meteorology, pollutant concentration and road traffic density predictors. The cross-correlation between continuous predictors is shown in Appendix I.

2.3. Regression learner

The Multilayer Perceptron Regressor (MLPR) available in the Phyton scikit-learn package has been used to fit the concentration of

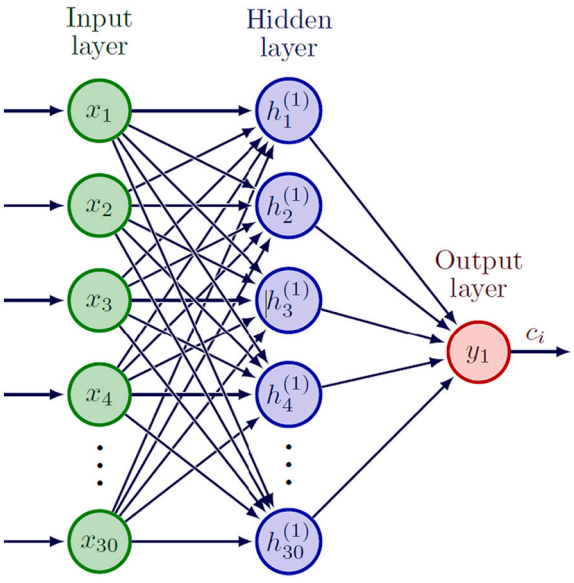

Fig. 2. Sketch of the MLPR showing an Input Layer and fully-connected layers with 30 neurons each and the single output layer containing the concentration of the species i, c_i.

all pollutant species using the predictors listed in Table 1 belonging to four categories: (i) meteorology, (ii) transportation intensity, (iii) the background particulate matter and (iv) one-hot-encoded variables for the station number, the hour of the day, the month of the year and the Low Emission Zone enforcement.

Hyperparameter tuning was done by comparing the results of the twelve network configurations resulting from trying three different depths (two, three and four layers) and 4 different number of neurons (10, 20, 30 and 40). Larger number of nodes or layers than those finally selected (2 layers with 30 neurons in the input and hidden layers) yielded marginally better fit scores during the training step at the cost of increased overfitting, this is, a significantly larger values of R^2 score in the training set in comparison to the test set. On the other hand, significantly reduced predictive accuracy was found for network configurations with less than 30 neurons.

The neural network, sketched in Fig. 2, is comprised of a 30-neuron input layer $x_1, \ldots, x_{30}$, each of them connected to all the predictor variables, followed by a fully-connected 30-neuron hidden layer $h_1^{(1)} \ldots h_{30}^{(1)}$ and a single output neuron y_1 containing the concentration prediction for pollutant i, c_i. The activation function is of the Rectified Linear Activation Function (RELU) type.

Model robustness has been assessed using a 5-fold cross-validation. The working dataset is randomly split in 5 folds and the model is trained using 4 of them, while the remaining data fold is used to test the fit performance by comparing the predicted values with the original values. The procedure is repeated 5 times using each of the data folds to test the fit performance. In order to reduce the variability of this estimation, the procedure is replicated a total of $q_r = 25$ times by randomly splitting the data into 5 subsets over which the 5-fold cross-validation procedure is applied resulting in q_r estimates of the pollutant concentration.

The training total CPU time is slightly above 2 h using a personal workstation equipped with 16Gb of RAM memory and a 6-core Intel i7–8700 chipset.

Learner performance is measured using the coefficient of determination R^2 defined, for each pollutant species, as

$$R^2 = 1 - \frac{SSres}{SStot} = 1 - \frac{\sum_{k=1}^{m} (c_k - \widehat{c}_k)^2}{\sum_{k=1}^{m} (c_k - \langle c \rangle)^2} \tag{4}$$

where *SStot* is the total sum of squares and *SSres* is the sum of residuals, c_k and $\hat{c}_k$ are the *k-th* observed and predicted value respectively and $\langle c \rangle$ is the averaged observed value.

2.4. Traffic monthly and daily averages

Human activity and mobility patterns are responsible for cyclic trends as shown in Fig. 3 that presents, from top to bottom, the monthly (left panels) and hourly (right panels) averages of road traffic density, number of vessels and number of flights at the Port and Airport of Barcelona. While road traffic and flight operations clearly intensify during daytime hours, port activity remains mostly constant over the 24-h period. On the yearly scale, summer vacation period explains the dip in both the road traffic and the port activity around August. Although noticeable, this increase in transportation activity during summertime in the case of air traffic is very modest.

The monthly (left panels) and hourly (right panels) average concentration for all pollutants is shown in Fig. 4. Each coloured dashed line corresponds to a different measuring station with the black line indicating the average across all stations. These profiles suggest that although there exists significant differences in the pollution levels between stations, the overall trend is very similar regardless of the specific location across the metropolitan area. The distinctive patterns in the average concentration for all pollutants suggests that the hour of the day and the month of the year along with the measurement station *id* should be used as predictors in training the model.

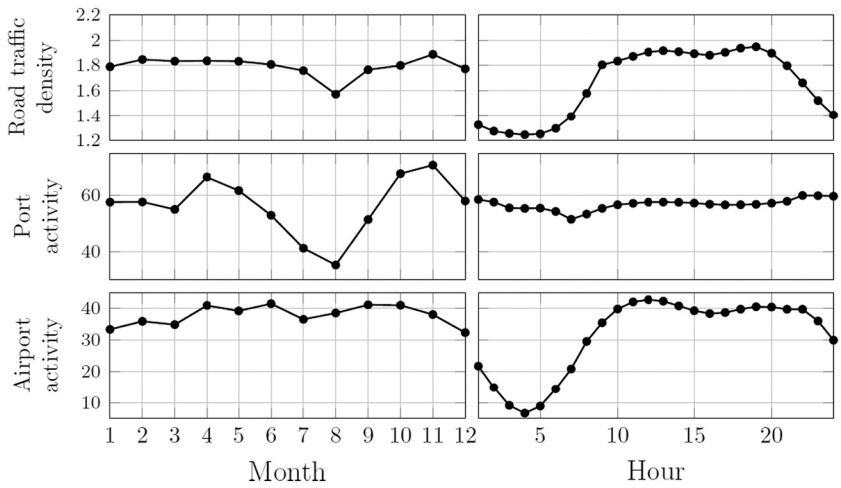

Fig. 3. From top to bottom: monthly (left) and daily (right) averages of Road traffic density, number of docked vessels at the Port of Barcelona, Port-station wind alignment, number of flight operations at the Airport of Barcelona and Airport-station wind alignment.

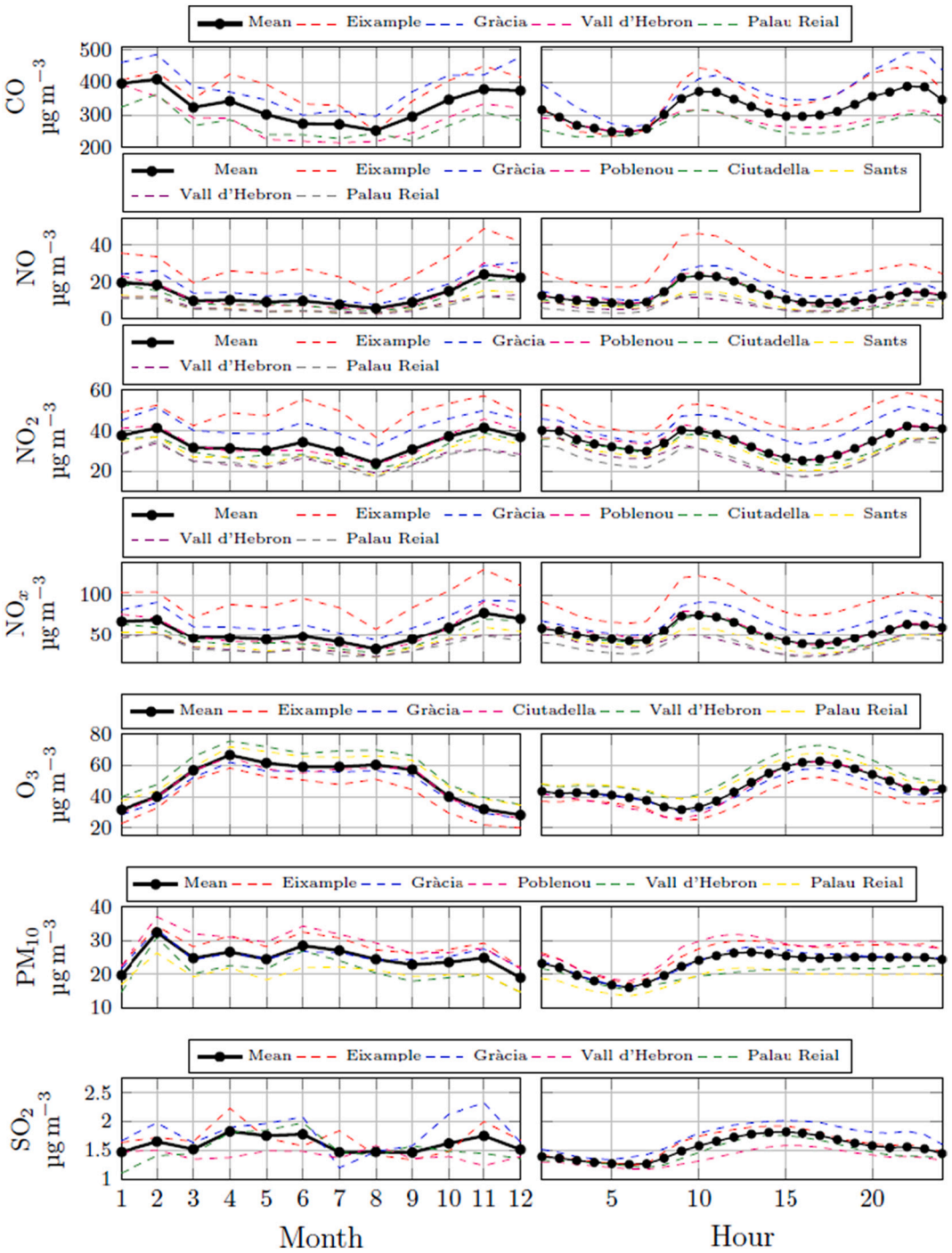

Fig. 4. From top to bottom: monthly (left) and daily (right) averaged concentration for each pollutant in $\mu g \cdot m^{-3}$ coloured by station. Black line shows the average across stations.

3. Results

3.1. Model accuracy performance

To illustrate the predictive capabilities of the data-based numerical model, Fig. 5 shows the measured and predicted NO_2 concentration in $\mu g \cdot m^{-3}$ between 1 January 2019 and 31 March 2019 for each measuring station reporting this pollutant.

The model accuracy in terms of the coefficient of determination R^2 for both the training and the test sets using the combined data from all $p = 7$ stations is listed in Table 2 for each pollutant species. The slightly higher values for the test set suggest that there is no overfitting of the data, indicating an appropriate choice of the MLPR configuration. The poorer values of performance for CO are very likely due to the notably lower number of observations for this species only available in 4 out of 7 measurement stations (see Appendix B). In the case of SO_2, in addition to this limitation in the number of data due to the lack of records at several measurement stations, the lower values of R^2 may be due to the limited resolution of the measurement instruments that record concentration values only as integers with a minimum value of 1. In the case of SO_2, which often presents very low concentration levels, this limitation could affect the predictive capability of the model.

For each pollutant, Table 3 lists common model evaluation statistics (Yu et al., 2006).

for the test set including the correlation coefficient (R^2), the fraction of predictions within a factor of two of observations (FAC2), the geometric mean bias (GeoMean) the geometric standard deviation (GeoSTD), the root-meansquare error (RMSE) and the mean bias (MeanBias). The last three rows include the same model accuracy metrics for the same three measurement stations (see Fig. 1) as reported by Benavides et al. *(*Benavides et al., *2019)* who used the operational mesoscale air quality forecast system CALIOPE-Urban v1.0 to predict the hourly NO_2 concentration. These results underline the potential of Machine Learning techniques in the prediction of pollutant concentrations in urban environments and their ability to provide concentration predictions as (or more) accurate than those

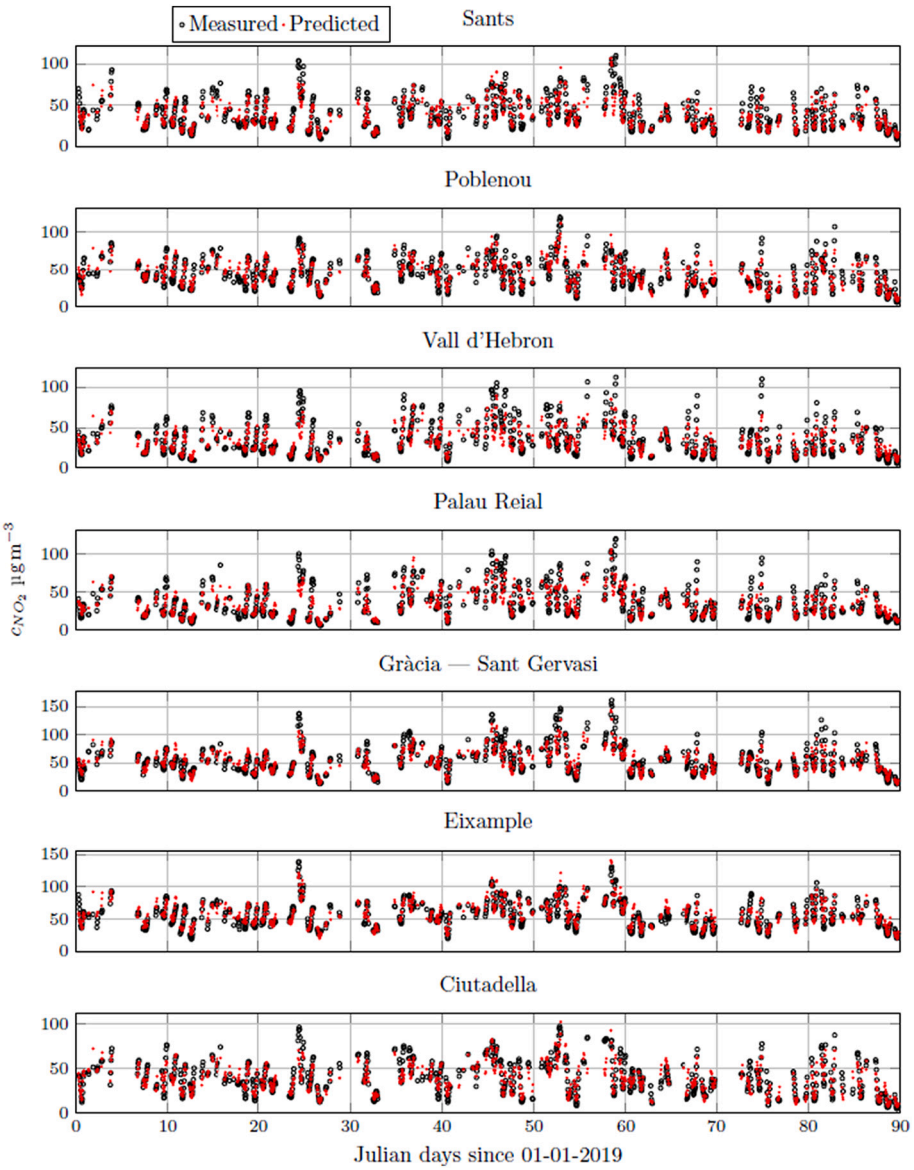

Fig. 5. Measured (empty black markers) and predicted (solid red markers) concentrations of NO_2 for each station over the first 90 days of 2019. (For interpretation of the references to colour in this figure legend, the reader is referred to the web version of this article.)

Table 2
Values of test and train R^2 for all pollutants.

Pollutant	Train R^2	Test R^2
CO	0.680	0.620
NO	0.839	0.809
NO_2	0.835	0.811
NO_x	0.838	0.813
O_3	0.857	0.819
PM_{10}	0.816	0.779
SO_2	0.651	0.583

Table 3
Model evaluation statistics for the test set for each pollutant including the correlation coefficient (R^2), the fraction of predictions within a factor of two of observations (FAC2), the geometric mean bias (GeoMean) the geometric standard deviation (GeoSTD), the root-mean-square error (RMSE) and the mean bias (MeanBias). The last three rows show the same model evaluation statistics for the same three measurement stations as reported by Benavides et al. *(*Benavides et al., *2019)* who used the operational mesoscale air quality forecast system CALIOPE-Urban v1.0 to predict the hourly NO_2 concentration.

Pollutant		R^2	FAC2	GeoMean	GeoSTD	RMSE	MeanBias
	PM_{10}	0.80	0.99	1.00	1.26	6.90	−0.90
	O_3	0.86	0.97	1.00	1.33	9.34	−1.53
	NO	0.76	0.87	1.00	1.60	11.76	−2.05
	NO_x	0.79	0.96	1.00	1.37	24.57	−3.81
	CO	0.64	0.99	1.00	1.27	110.40	−12.71
	SO_2	0.64	0.99	1.00	1.28	0.58	−0.08
	NO_2	0.82	0.99	1.00	1.29	8.91	−1.26
	Palau Reial	0.32	0.73	1.10	1.22	21.6	−1.23
NO_2 (Benavides et al., 2019)	Eixample	0.31	0.86	0.83	1.11	26.7	−8.57
	Gr'acia	0.28	0.79	1.07	1.19	25.1	6.00

obtained with state-of-the-art physics-based methodologies.

3.2. Feature importance

The importance of each standardised feature in a linear (or generalised linear) model can be directly assessed by comparing the magnitude of each regression coefficient. In contrast, the contribution of each feature to the response variability in non-linear models requires alternative approaches. The Permutation Feature Importance (PFI) method (Wei et al., 2015; Breiman, 2001), agnostic with respect to both the model and the score function, estimates the importance of each predictor by calculating the decrease in the model prediction score after randomly permuting the values of this predictor. A predictor is 'important' if shuffling its values decreases the model score and it is 'unimportant' otherwise. As predictors are shuffled (several times and averaged), the fraction of response variability explained by the model decreases resulting in scores below the 'best' value attained before shuffling. This descent in the R^2 score is not bounded and can attain negative values when the prediction is worse than predicting just the mean of the fitted variable. To be consistent with the rationale beyond the method and the nature of the data used here, there are four predictors (*wind_dirx*, *wind_diry*, *alig_port* and *alig_aero*) that are shuffled simultaneously because all of them are derived from the wind direction, which is a primitive variable that enters into the model through these four feature-engineered variables. Their joint effect is included in the plots with the label *wind_alig*. The PFI results, shown in Appendix J, suggest that most pollutant concentration variability is affected by the temporal predictors and the local position within the metropolitan area (accounted via the measurement station code). Temperature is also found to be a relevant predictor for PM_{10} and SO_2.

3.3. Transportation emissions impact

The individual impact of each predictor associated with transportation is determined by adding a perturbation δx_j to the observed predictor value x_j for each observation in the working data set and taking the mean value of the predicted concentration $\langle c \rangle$ over all observations while holding the other predictors at their respective observed values. The results are shown in Fig. 6 where the x-axis contains the normalized perturbation defined as

$$\Delta x_j = 100\,\frac{\delta x_j}{x_j} \tag{5}$$

while the average prediction for each species i over all observations, $\langle c_i \rangle$, belongs on the *y*-axis. The excellent predictive capabilities of the model ensure that the predicted concentration at $\Delta x_j = 0$ are very close to the observed values. Red thick lines show a line with the slope at $\Delta x_j = 0$, this is, the rate of change in concentration in the vicinity of the observed value.

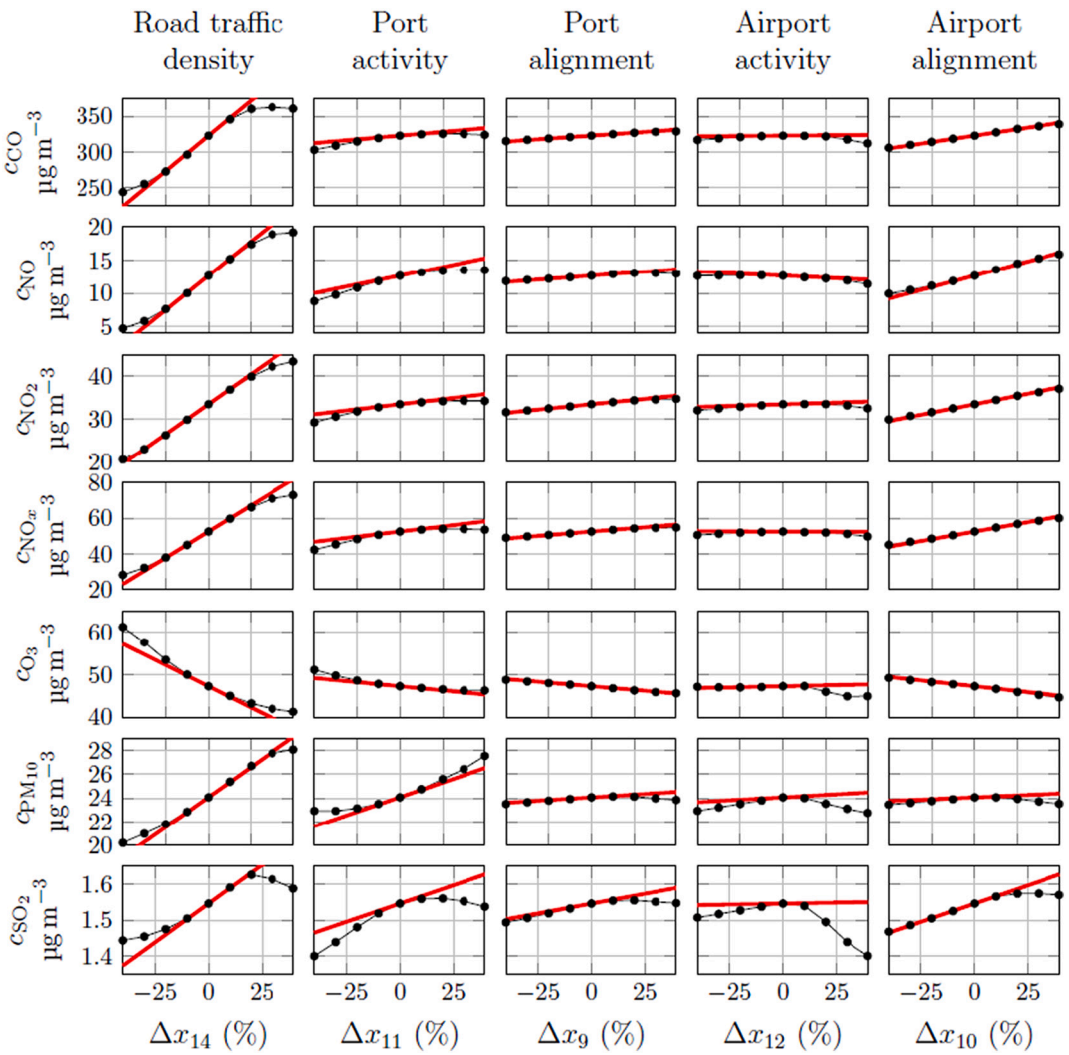

Fig. 6. Average predicted dependence of pollutant concentration on each transportation predictor intensity. From left to right columns: Road traffic density, Port activity, Port wind alignment, Airport activity and Airport wind alignment. Thick red lines indicate the slope at $\Delta x_j = 0$. (For interpretation of the references to colour in this figure legend, the reader is referred to the web version of this article.)

Keeping in mind the definitions of each transportation predictor, either as a measure of traffic density expressed on a 1 to 5 scale or as the number of docked vessels or flight movements, results suggest that the road traffic density is the predictor with the largest impact on the pollutant concentrationfor all considered chemical species. The dependence of the concentration on variations of the road traffic density (expressed as a percentage with respect to the observed value) is mostly linear across the ±40% range shown in Fig. 6. Notably, as $|\Delta x_{14}|$ increases, model predictions linearity decreases resulting in milder changes in NO_2 concentration for larger variations in the predictor. This apparent saturation of the prediction may be due to the fact that as Δx_j increases, the number of extreme predictor values used to train the model decreases.

Although notably smaller in comparison to road traffic, results suggest that the number of vessels (used as a proxy for Port emissions) has also a significant impact on pollutant concentration levels in the metropolitan area. In contrast, the number of flight operations (used as a proxy for Airport activity) seem to have a very modest contribution to worsened Air Quality. It is worth mentioning that while the Port of Barcelona is located within the metropolitan area of the city, the Airport of Barcelona is located more than 10 km from the city center (see Fig. 1).

All these results are in agreement to the estimated NO_x emission share per sector in the city of Barcelona reported in the Urban NO_2 Atlas elaborated by the European Commission (Degraeuwe et al., 2019b) that attributes a negligible contribution of the air traffic to this pollutant total emissions. In the same report, road traffic and shipping activities are estimated to contribute with approximately half and a quarter of the total NO_x emissions respectively. The remaining 25% of emissions correspond to residential and industrial sources.

Notably, except for PM_{10}, the wind alignment with respect to the Airport has a larger effect on the pollutant concentration than the

number of flight operations. This could be the explained by the presence of industrial sites in between the Airport of the metropolitan area of Barcelona (see Fig. 1). The model could be 'learning' that while the air traffic intensity does not contribute significantly to the local Air Quality, when the wind blows from the Airport direction towards the city, pollutant concentrations increase due to emissions released in between the Airport and the measuring station.

The relative lack of robustness of the SO_2 predictions can be explained by the very small variability in its concentration that ranges between approximately 1.45 and 1.65 $\mu g \cdot m^{-3}$ and, more importantly, by the limitations of the station measurement equipment capable only of reporting concentration (in $\mu g \cdot m^{-3}$) using integers. SO_2 concentration values near or below unity will result in an unrealistically high frequency of 1 $\mu g \cdot m^{-3}$ records that will degrade the accuracy of the model in predicting the concentration of this particular pollutant under low concentration scenarios.

The individual impact of each transportation mode is summarized in Table 4 that presents the normalized ratio of the variations in the response and the predictor defined as

$$m_j = \frac{\Delta\langle c\rangle/\langle c\rangle}{\delta x_j/x_j} \tag{6}$$

where $\Delta\langle c\rangle$ is the variation in the average concentration as a response to changes of magnitude δx_j in the corresponding predictor. In addition, the non-normalized version of this slope, defined as

$$\widetilde{m}_j = \frac{\Delta\langle c\rangle}{\delta x_j} \tag{7}$$

is also included in parenthesis for each transportation mode.

It is crucial to note that all three transportation predictors have a very different definition. While the number of docked vessels and the number of flight operations are naturally related to the number of units of each class in each respective infrastructure, the road traffic density predictor is a normalized quantity bounded between the values of 1 and 5 corresponding to 'very fluid' and 'congested' conditions respectively. Moreover, the number of docked vessels and flight operations are respectively assumed to be correlated to each facility total emissions.

The units of $\widetilde{m}_j$ should therefore be read as an increment of concentration of $\mu g \cdot m^{-3}$ (i) per point of traffic density in the 1 to 5 range, (ii) per increased Port emissions expressed as an additional docked vessel at the Port of Barcelona and (iii) per increased Airport emissions expressed as an additional flight operation at the Airport of Barcelona.

As already shown in Fig. 6, the road traffic density, as defined in this work, has the largest impact on increased pollutant concentration. Every increase in one unit of road traffic density is estimated to be responsible for a variation of 137.91, 14.19, 19.34, 40.50, −14.18, 6.98 and 0.24 $\mu g \cdot m^{-3}$, of CO, NO, NO_2, NO_x, O_3, PM_{10} and SO_2 respectively. Likewise, the change in the overall Port activity associated with an additional docked vessel at the Port of Barcelona at a given hour is estimated to change the concentration of the same pollutants by 0.46, 0.11, 0.10, 0.25, −0.08, −0.11 and 0 $\mu g\ m^{-3}$ respectively. Pollutant concentration variations due to changes in the Airport activity represented by an additional flight operation per hour at the Airport of Barcelona are below 0.06 $\mu g\ m^{-3}$.

To illustrate the impact of wind alignment and velocity, the values of m_j for these predictors are also shown. Results suggest that a better alignment of the wind with respect to the Port of Barcelona, as defined in Eq. (2), has the largest impact on the nitrogen oxides concentration. Despite the negligible impact of the Airport activity, the wind alignment with respect to the Airport seems to be larger than that for the Port. As mentioned before, a plausible explanation is related to the existence of industrial sites in between this infrastructure and the metropolitan area. On the other hand, the decrease in pollutant levels as wind velocity increases could be explained by the enhanced turbulent mixing due to larger wind shear within the urban canopy.

3.4. Low Emission Zone impact

The impact of the Low Emission Zone on the pollutant concentration is shown in Fig. 7 that plots the predicted difference in

Table 4
Ratio between the relative rate of change of each mean pollutant concentration and the relative rate of change of each variable m_j. For each transportation mode the non-normalized value $\widetilde{m}_j$ is shown in parenthesis.

Predictor	CO	NO	NO_2	NO_x	O_3	PM_{10}	SO_2
Road Density	0.76	2.03	1.05	1.40	−0.53	0.53	0.28
	(137.91)	(14.19)	(19.34)	(40.50)	(−14.18)	(6.98)	(0.24)
Port activity	0.08	0.52	0.18	0.27	−0.10	0.26	0.13
	(0.46)	(0.11)	(0.10)	(0.25)	(−0.08)	(−0.11)	(0.00)
Airport activity	0.01	−0.12	0.05	−0.01	0.02	0.04	0.01
	(0.06)	(−0.04)	(0.04)	(−0.01)	(0.03)	(0.03)	(0.00)
Port alignment	0.06	0.19	0.15	0.19	−0.09	0.05	0.07
Airport alignment	0.14	0.68	0.29	0.40	−0.12	0.03	0.13
Wind velocity	−0.15	−0.45	−0.23	−0.33	0.23	0.02	−0.06

pollutant concentration under the LEZ with respect to the unrestricted traffic, Δc_i. The boxplots show the distribution over the q_r numerical experiments where the centerline, the box and the whiskers represents the median, the Interquartile Range and the minimum (lower whisker) and maximum (upper whisker) values of the distribution.

Results suggest that the LEZ has a statistically significant impact on the carbon monoxide and nitrogen oxides concentration achieving a mean reduction of approximately 8.0, 2.5, 4.0 and 8.0 $\mu g \cdot m^{-3}$ for CO, NO, NO_2 and NO_x respectively.

With a mean concentration value of NO_x before the LEZ implementation of 54 $\mu g \cdot m^{-3}$, this traffic restriction measures are therefore predicted to abate the total NO_x levels by approximately 15%. Regarding each individual nitrogen oxide, reductions in NO_2 and NO are predicted to be 12% and 13% respectively. Although larger in magnitude in comparison to nitrogen oxides, the difference in CO concentration before and after the LEZ would result in a 2.5% reduction in the concentration of this pollutant with respect to its mean value.

Regarding the other pollutants levels, results in Fig. 7 suggest that the LEZ has no significant impact on the concentration of ozone, suspended particulate matter and sulfur dioxide.

The impact of the LEZ measures on the Air Quality in the metropolitan area of Barcelona, predicted here to result in a 12% reduction in NO_2 concentration, is found to be negligible in the first report published by the Barcelona Public Health Agency (ASPB in Catalan). This report concluded that, although the implementation of LEZ sanctions starting in September 2020 prompted a significant renewal of the vehicle fleet and a consequent decrease in the share of the most polluting cars, the restriction measures did not result in significant decreases in NO_2 concentration levels across the metropolitan area (Grup d'Avaluació de l'Impacte de la Zona de Baixes Emissions ZBE Rondes Barcelona, 2021). The improvement in the Air Quality observed during 2020 was explained by the mobility abatement due to the COVID-19 pandemic lockdown with no contribution attributable to the deployment of the LEZ measures. The report concluded that a proper analysis of the LEZ impact required longer-term data, especially in the COVID-19 context with unusual mobility patterns. In addition, it was stated that further Air Quality improvements should be expected as restrictive measures affect more vehicle types in the coming months.

The discrepancy with the current results is due to the methodology used in the ASPB report, which consists of a mere comparison of the average NO_2 reduction between the metropolitan area within the LEZ boundaries (see map in Fig. 1) and two control zones, one extending over the metropolitan belt (near field) and the other further away that includes large rural areas. By comparing the concentration levels in these three regions during three stages (1) the Spring 2020 lockdown, (2) the Summer 2020 'new normality' and (3) the Autumn 2020 new restrictions, the authors did not find significant differences between the LEZ-affected domain and the outer control regions. Concentration variability due to meteorology was accounted using an unspecified and non-referenced methodology.

Importantly, a second report by the Barcelona City Council (Departament d'Avaluació i Gestió Ambiental, 2022) presented the results of a model predicting a reduction of 18.1% in the NO_2 concentration as a result of the LEZ measures with respect to values in 2017 at one single location corresponding to the measurement station with the highest pollutant concentration. Therefore, this second report predicts a reduction in NO_2 concentration that is of the same order as the 12% reduction in this pollutant predicted in the present work across the entire metropolitan area.

The impact of the Barcelona LEZ on the NO_x concentration was also estimated using the CALIOPE-Urban model (Benavides et al., 2019; Benavides et al., 2020) who reported a reduction of 13.1% in NO_x concentration (Rodriguez-Rey et al., 2022), a value that is very close to the 15% estimated in the present work.

4. Discussion

While physics-based models require detailed emission inventories for each pollutant to define the source terms in the transport equations, the present data-driven methodology has been found to accurately predict pollutant concentrations using only readily available predictors of traffic intensity for each transportation mode. Using Machine Learning techniques, the resulting model can be used to assess the impact on Air Quality due to changes in each individual pollutant contributor. Thus, the effectiveness of mitigation

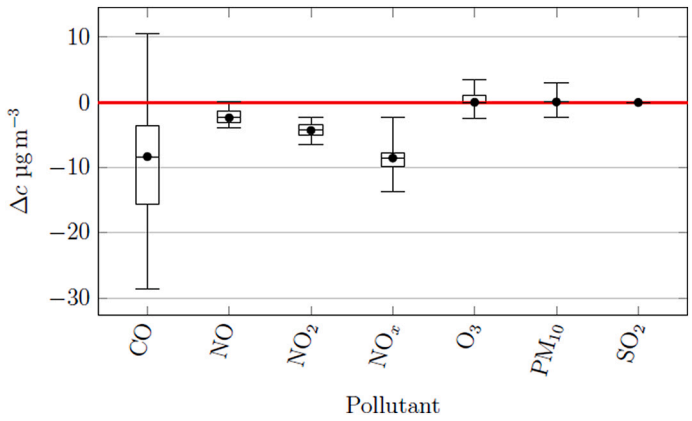

Fig. 7. Predicted concentration reduction in $\mu g \cdot m^{-3}$ associated to the Low Emission Zone restriction measures on road traffic for each pollutant.

measures that restrict the type of vehicles accessing the city of Barcelona has been evaluated by estimating the reduction in concentration due exclusively to their enforcement.

A key assumption in the present methodology is that the traffic density reported by the City Council of Barcelona is an appropriate surrogate for the amount of pollutant emissions from fossil fuel-based vehicles. In a similar way, (i) the number of docked vessels at the Port of Barcelona is used here as a proxy for overall Port activity emissions that include emissions from ships but also from logistics operations, service vehicles, etc. and (ii) the number of flight operations is assumed to represent the overall emissions in the Airport of Barcelona, that, besides those emitted by aircraft, may include also maintenance operations, taxing, etc. All in all, it is assumed here that all these surrogates are correlated to the overall emissions for each transportation mode.

Future improvements to the model will depend on the availability of "finer-grained" data that will facilitate better characterization of the emissions inventory that may come, for example, from road traffic intensity data broken down by vehicle type. Of course, adding predictors to explicitly account for residential, industrial, energy production and agriculture emissions could further improve the current model predictive capabilities increasing also the flexibility of the present methodology to investigate other metropolitan areas with distinct emission shares by sector.

It should also be noted that, by considering all measurement station data combined, the present results can be regarded as a overall prediction of the pollutant concentration across the entire metropolitan area. Of course, individual models can be used for each station if separate predictions for each location in the metropolitan area are required. In this sense, the availability of concentration predictions only for locations for which data exist could be considered as a limitation of the methodology presented here, in contrast to classical physics-based models that typically provide pollution level maps over the entire computational domain.

5. Conclusions

The present work demonstrates that it is possible to use Machine Learning/Artificial Intelligence techniques to obtain very accurate predictions of local pollutant concentrations with modest CPU resources without requiring detailed information on usually unavailable variables including local atmospheric hydrodynamics, surface heat flux, emission inventories of different types including mobile sources and urban layouts. In comparison to physics-based CALIOPE-Urban v1.0 model, the present data-based approach has demonstrated better performance in predicting local concentration of NO_2 at selected locations in the city of Barcelona using readily available datasets from Open Data repositories.

Using data between October 2017 and June 2021, the dependence between the concentration levels of CO, NO, NO_2, NO_x, PM_{10}, O_3 and SO_2 on (i) local meteorology, (ii) road traffic density, (iii) number of docked vessels at the Port and (iv) number of flight movements at the Airport have been obtained using a Multilayer Perceptron Regressor. The resulting model has been used to estimate the individual impact of each transportation mode on pollutant levels in the metropolitan area exploiting the unexpected opportunity of the COVID-19 pandemic lockdown to train Machine Learning models with unusually low values of transportation intensity. Predictive performance for each pollutant in terms of R^2 range between 0.58 and 0.82.

Under the definition of the transportation predictors, results suggest that road traffic has the greatest influence on pollutant concentration, followed by maritime traffic. Compared to these two, air traffic was found to barely contribute to worsened Air Quality. For instance, road, maritime and air traffic are estimated to be responsible for an increase in NO_2 concentration of 1.05, 0.18 and 0.04 percentage points per percentage point increase on each predictor.

When used to investigate the impact of the Low Emission Zone mitigation measures aimed at improving the Air Quality in the metropolitan area of Barcelona, the present model results are in good agreement with both the Barcelona City Council predictions and the estimations from a state-of-the- art physics-based model. The present analysis suggests that the road traffic restrictions that began in September 2020 are responsible for a 15% reduction in total nitrogen oxides concentration. Although significant decreases in carbon monoxide levels are also predicted, other pollutants such as particulate matter and sulfur dioxide appear to be unaffected by this mitigation measure.

Future extensions of the present work will be directed at improving the present predictive capabilities by adding better urban mobility predictors and use power consumption per sector as a proxy to account for residential and industrial emissions.

CRediT authorship contribution statement

Alexandre Fabregat: Methodology, Software, Validation, Formal analysis, Investigation, Data curation, Writing – original draft, Visualization, Funding acquisition. **Anton Vernet:** Conceptualization, Methodology, Validation, Formal analysis, Investigation, Supervision, Writing – review & editing, Project administration, Funding acquisition. **Marc Vernet:** Validation, Formal analysis, Investigation. **Lluís Vázquez:** Conceptualization, Methodology, Validation, Writing – review & editing, Project administration, Funding acquisition. **Josep A. Ferŕe:** Conceptualization, Methodology, Validation, Formal analysis, Investigation, Supervision, Writing – review & editing, Project administration, Funding acquisition.

Declaration of Competing Interest

All authors declared no conflicts of interest.

Data availability

Data will be made available on request.

Acknowledgments

This work has been funded by Spanish Ministerio de Ciencia, Innovación y Universidades through the grants DPI2016-75791-C2-1-P and RTI2018- 100907-A-I00 (MCIU/AEI/FEDER, UE) and also by the Generalitat de Catalunya through the grant 2017-SGR-1234.

The authors thank (i) The European Organisation for the Safety of Air Navigation (EUROCONTROL) and Bruno Nicolas for providing the data on air traffic at the Airport of Barcelona and (ii) the Open Data BCN portal for their efforts in maintaining and sharing an outstanding collection of datasets.

Appendix A. Imputation of the road traffic data from March to May 2020

The road traffic density dataset in the metropolitan area of Barcelona (Open Data BCN, 2022a) exhibits an interruption between March 16th and June 4th 2020. Since the working dataset is only comprised of complete hourly observations (i.e., observations for which all predictors exists), this 1932 h long gap would propagate during the table merging. Missing data imputation on traffic density was carried out using an alternative dataset on metropolitan mobility, namely, the 'mobility capacity' dataset also available at the Open Data BCN portal (Open Data BCN, 2022b).

Support Vector Regression (SVR) is a popular technique in Supervised Learning non-linear problems in a wide range of applications (*Energy*, 2014; Shamshirband et al., 2015). Using Python scikit-learn SVR (Sklearn package-SVR, 2022) was used to fit the original traffic density data (expressed in a 1–5 scale) to the 'mobility capacity' dataset containing the average number of vehicles per day. While the sampling rate of the traffic density data is hourly, mobility data came as daily averages by weekday. In addition, each dataset was generated with measurements taken from a different station networks lacking of spatial collocation.

First, mobility and traffic density data were expressed on the same temporal axis by averaging the hourly traffic measurements to weekly values for each month. For each traffic station, the set of the 10 nearest mobility measurement locations was identified allowing for estimations of daily average traffic intensity. Since mobility data was expressed in weekdays, separate models were used to imputate the original data set using predictions of the hourly traffic value based on the daily average and the hour of the day.

Appendix B. List of pollutant measuring stations

The list of pollutant measurement stations and data availability for each pollutant species is shown in Table B.5.

Table B.5
Pollutant measurement station type and data availability for each species. 'BU' stands for *Background Urban* and 'TU' for *Traffic Urban*.

Station name	Type	CO	NO	NO_2	NO_x	O_3	PM_{10}	SO_2
Poblenou	BU	–	✓	✓	✓	–	✓	–
Sants	BU	–	✓	✓	✓	–	–	–
Eixample	TU	✓	✓	✓	✓	✓	✓	✓
Gr'acia-Sant Gervasi	TU	✓	✓	✓	✓	✓	✓	✓
Ciutadella	BU	–	✓	✓	✓	✓	–	–
Parc Vall Hebron	BU	✓	✓	✓	✓	✓	✓	✓
Palau Reial	BU	✓	✓	✓	✓	✓	✓	✓

Appendix C. Background levels of PM_{10}

The map in Fig. C.8 depicts the location of the rural pollutant concentration measurement station near the town of Sort.

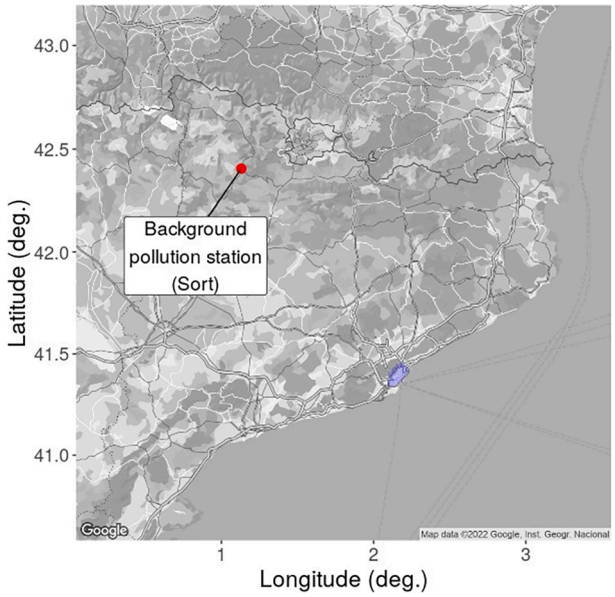

Fig. C.8. Locations of the metropolitan area of Barcelona (blue overlay) and the rural pollutant concentration measurement station (red marker) used to obtain background levels of PM_{10}. (For interpretation of the references to colour in this figure legend, the reader is referred to the web version of this article.)

Appendix D. Meteorology stations

The map in Fig. D.9 depicts the location and identifiers of the two meteorological stations within the metropolitan area of Barcelona.

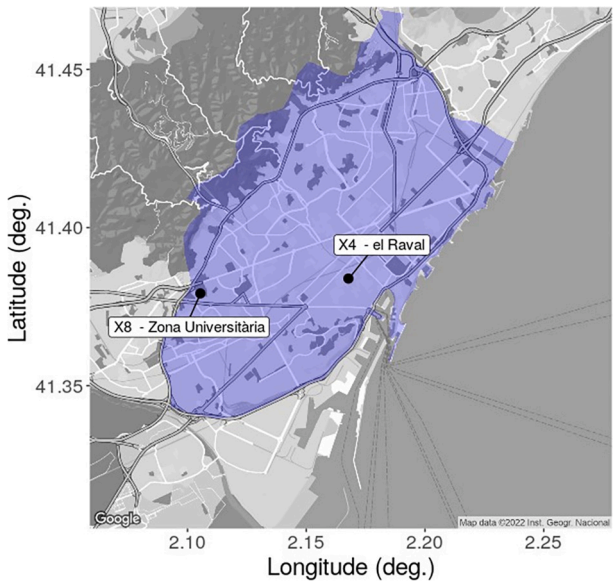

Fig. D.9. Location and identifiers of the two meteorological stations within the metropolitan area of Barcelona (blue overlay). (For interpretation of the references to colour in this figure legend, the reader is referred to the web version of this article.)

Appendix E. Meteorology

To illustrate the meteorological data (Servei Meteorològic de Catalunya Catalan Meteorologic Service, 2022), Fig. E.10 shows the temporal evolution of several key predictors for the year 2020 as recorded by a measurement station located in the metropolitan area of Barcelona. Note that the zero angle for the wind direction in Fig. E.10 points to the North and increases in the anticlockwise direction. Signal interruptions are due to maintenance or malfunction of the station measurement equipment.

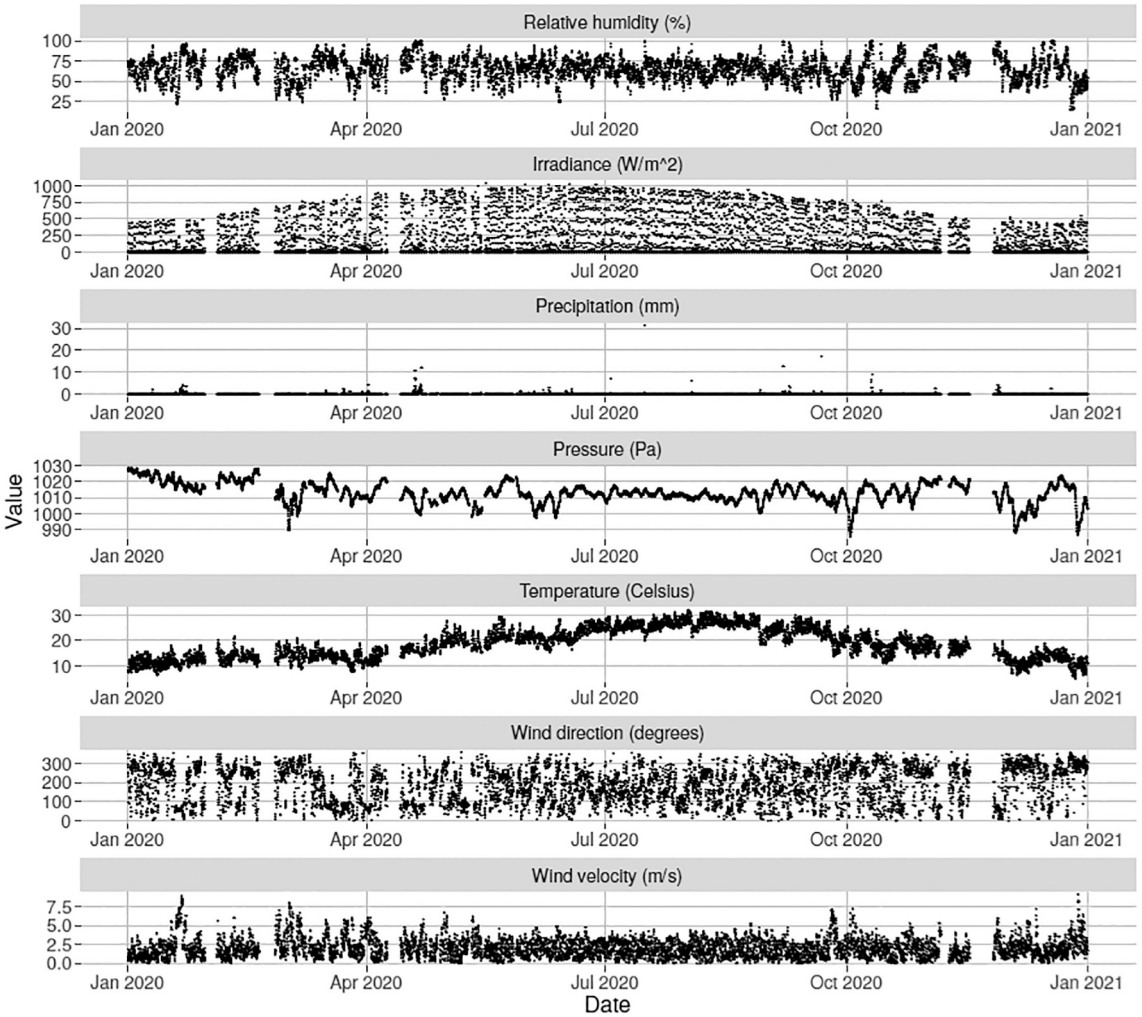

Fig. E.10. Temporal evolution of meteorologic predictors over 2020. From top to bottom: relative humidity (%), irradiance (W m^{-2}), precipitation (mm), pressure (hPa), temperature (°C), wind direction (°) and wind velocity (m s^{-1}).

Appendix F. Airport of Barcelona activity

The temporal evolution of the Airport of Barcelona activity between February and April 2020 is shown in Fig. F.11. The colour indicates the flight time (either arrival or departure). The impact of the COVID-19 pandemic lockdown, initiated on March 14, 2020 (red dashed vertical line), resulted in a notable reduction in the hourly number of airport movements that fell from a typical peak value of around 60 to less than 10 by March 25, 2020.

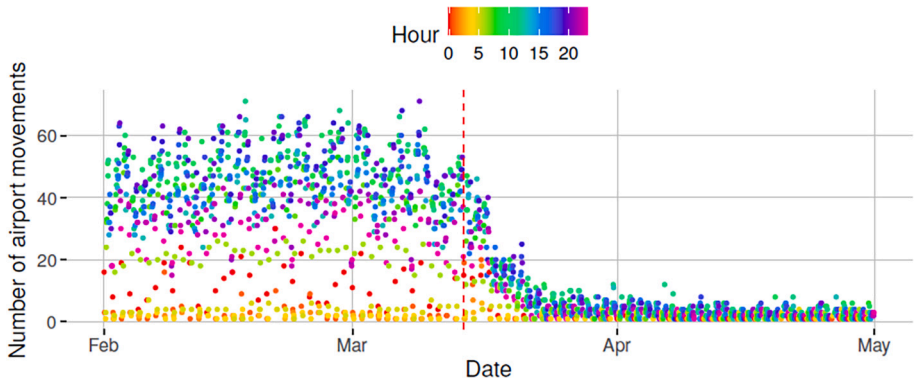

Fig. F.11. Number of hourly movements at the Airport of Barcelona between February 2020 and April 2020. Colour indicates the hour of the day. The initialization of national lockdown in Spain on March 14, 2020 is shown as a vertical dashed red line. (For interpretation of the references to colour in this figure legend, the reader is referred to the web version of this article.)

Appendix G. Port of Barcelona activity

The number of hourly total vessels docked at the Port of Barcelona between January 2019 and December 2020 is shown in Fig. G.12. The colour corresponds to percentage of total vessels that are cruise liners. As it happened for the air traffic (see Fig. F.11), the initialization of the pandemic lockdown in Spain on March 2020 (shown as a gray vertical line) led to a marked decrease in the overall Port activity. This reduction is especially pronounced in the number of cruise liners movements.

The distributions of the length of stay at dock in hours for the cruise liners and all vessels are shown in Fig. G.13. Most cruise liners spent around 12 h at the Port of Barcelona.

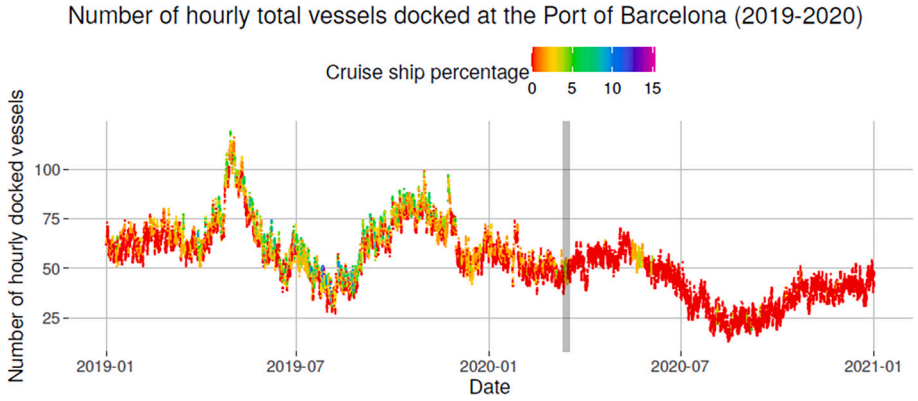

Fig. G.12. Number of hourly total vessels docked at the Port of Barcelona between January 2019 and December 2020. Colour indicates the fraction of vessels that are cruise liners.

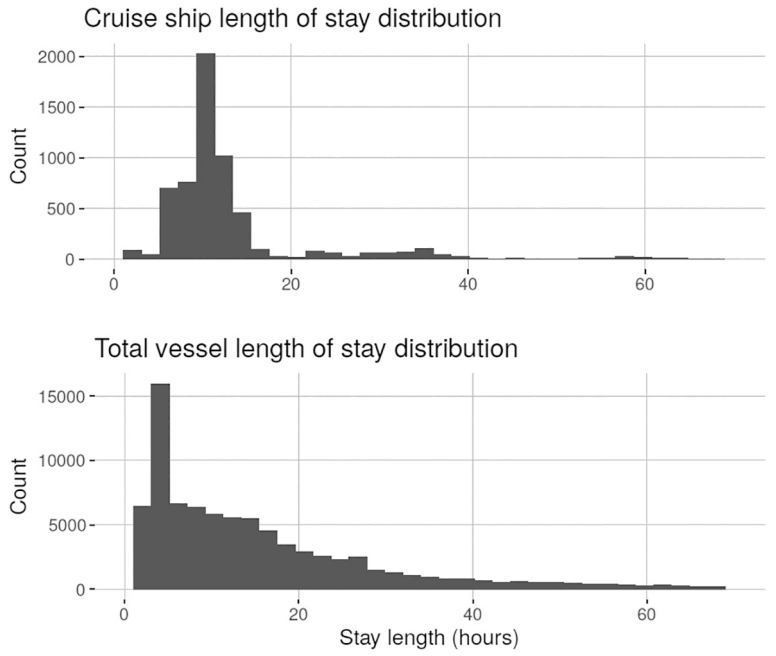

Fig. G.13. Top panel: Distribution of the length of stay in hours at the Port of Barcelona for cruise liners. Bottom panel: same for all vessels.

Appendix H. Low Emission Zone

The vehicles affected by the Low Emission Zone in Barcelona (Grup d'Avaluació de l'Impacte de la Zona de Baixes Emissions ZBE Rondes Barcelona, 2021), launched in January 2020 but operational in practice since September 2020 when ticketing started, are:

- Petrol cars pre-Euro 3 (usually registered before 2000) and diesel cars before Euro 4 (usually pre-2005 or 2006).
- Motorcycles and mopeds before Euro 2 (usually registered before 2003).
- Vans, trucks and buses without an environmental label which have been progressively affected as follows:
  - From 1 April 2021, petrol vans pre-Euro 3 petrol (usually registered before 2000) and diesel vans pre-Euro 4 standard (usually registered before 2005 or 2006).
  - From 1 January 2022, trucks and small coaches prior to the Euro 4 standard (usually registered before 2006 or 2007).
  - From 1 July 2022, buses and coaches intended for public transport prior to the Euro 4 standard (usually registered before 2006 or 2007).

Appendix I. Feature cross-correlation

The cross-correlation value between the numerical (non-categorical) predictors is shown in Fig. I.14.

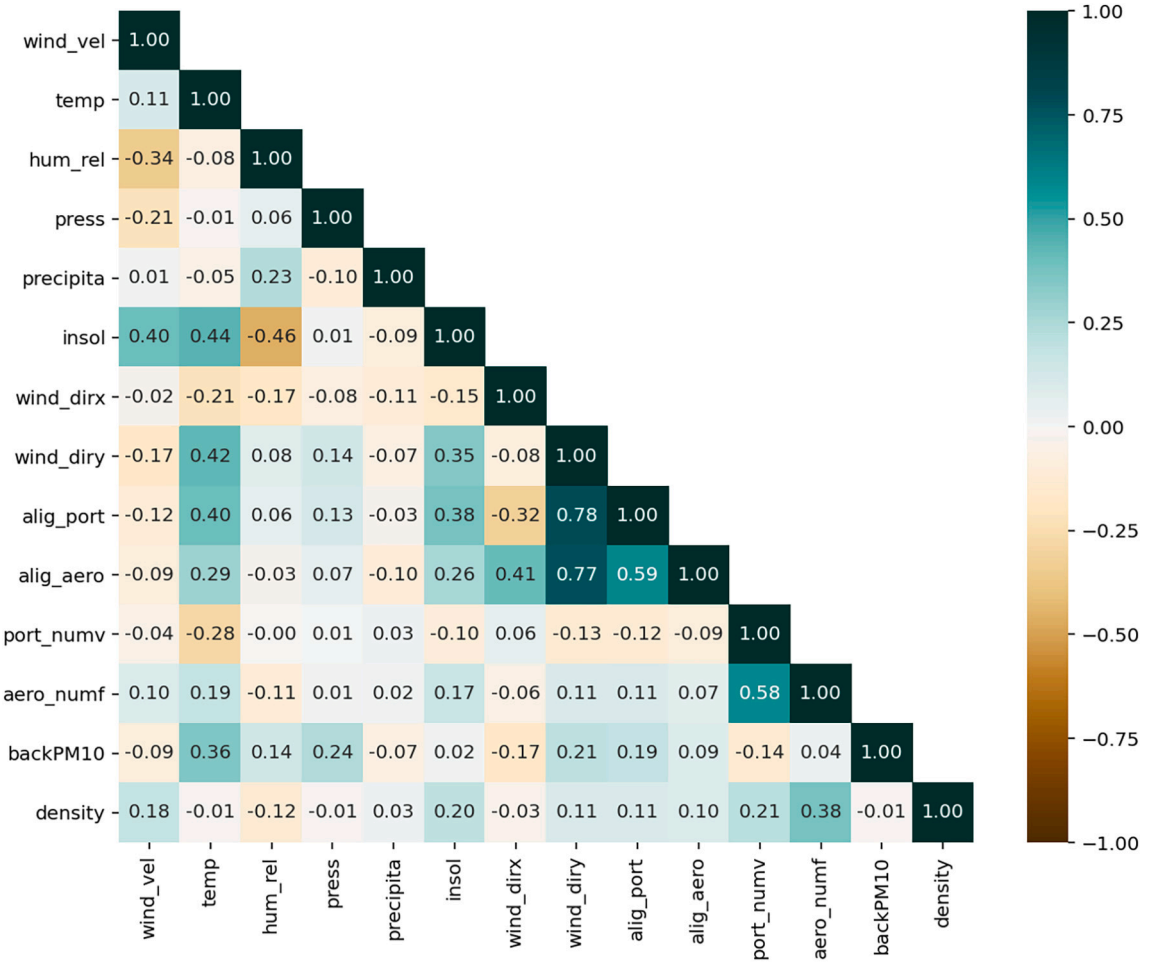

Fig. I.14. Cross-correlation coefficients for the non-categorical predictors.

Appendix J. Permutation feature importance results

The results for the Permutation Feature Importance (PFI) for all pollutants are shown in Fig. J.15. No permutation and full permutation are shown in red and blue lines respectively. The larger the decrease in the permuted case with respect to the non-permuted, the larger the impact of that predictor on the correlation coefficient R^2.

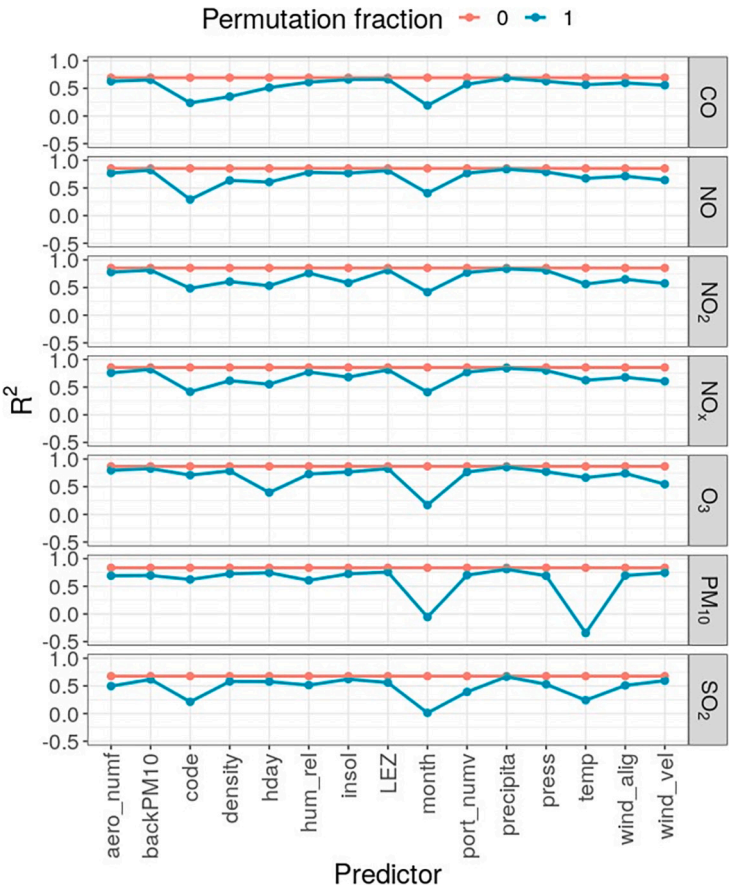

Fig. J.15. Permutation Feature Importance for all pollutants. The two curves correspond to no permutation (in red) and full permutation (in blue). (For interpretation of the references to colour in this figure legend, the reader is referred to the web version of this article.)

References

Arnaudo, E., Farasin, A., Rossi, C., 2020. A comparative analysis for air quality estimation from traffic and meteorological data. Appl. Sci. 10, 4587.

B, M., 2010. How much, how long, what, and where: air pollution exposure assessment for epidemiologic studies of respiratory disease. Proc. Am. Thorac. Soc. 7 (2), 111–115.

Beevers, S., Kitwiroon, N., Williams, M., Kelly, F., Anderson, H., Carslaw, D., 2013. Air pollution dispersion models for human exposure predictions in London. J. Expos. Sci. Environ. Epidemiol. 23 (02).

Benavides, J., Snyder, M., Guevara, M., Soret, A., Garcıa-Pando, C. Perez, Amato, F., Querol, X., Jorba, O., 2019. CALIOPE-Urban v1.0: coupling R- LINE with a mesoscale air quality modelling system for urban air quality forecasts over Barcelona city (Spain). Geosci. Model Dev. 12 (7), 2811–2835. URL. https://gmd.copernicus.org/articles/12/2811/2019/.

Benavides, J., Soret, A., Guevara, M., Garcıa-Pando, C. Perez, Snyder, M., Amato, F., Querol, X., Jorba, O., 2020. Potential impact of a low emission zone on street-level air quality in Barcelona City using CALIOPE. Urb. Mod. 171–176.

Breiman, L., 2001. Random forests. Mach. Learn. 45, 5–32.

Byun, D., Schere, K., 2006. Review of the governing equations, computational algorithms, and other components of the Models-3 community multiscale air quality (CMAQ) modeling system. Appl. Mech. Rev. 59, 51–77.

Castelli, M., Clemente, F., Popovic, A., Silva, S., Vanneschi, L., 2020. A machine learning approach to predict air quality in California. Complexity 1–23.

Chau, P.N., Zalakeviciute, R., Thomas, I., Rybarczyk, Y., 2022. Deep learning approach for assessing air quality during COVID-19 lockdown in Quito. Front. Big Data 5.

Cohen, A., Erson, H., Ostra, B., Pandey, K., Krzyzanowski, M., Kunzli, N., Gutschmidt, K., Pope, C., Romieu, I., Samet, J., 2006. The global burden of disease due to outdoor air pollution. J. Toxicol. Environ. Health Part A 68, 1–7.

Cohen, A., Brauer, M., Burnett, R., Anderson, H., Frostad, J., Estep, K., Balakrishnan, K., Brunekreef, B., Dandona, L., Dandona, R., Feigin, V., Freedman, G., Hubbell, B., Jobling, A., Kan, H., Knibbs, L., Liu, Y., Martin, R., Morawska, L., Forouzanfar, M., 2017. Estimates and 25-year trends of the global burden of disease attributable to ambient air pollution: an analysis of data from the global burden of diseases study 2015. Lancet 389, 1907–1918.

Degraeuwe, B., Pisoni, E., Peduzzi, E., De Meij, A., Monforti-Ferrario, F., Bodis, K., Mascherpa, A., Astorga-Llorens, M., Thunis, P., Vignati, E., 2019a. Urban NO2 Atlas, iSBN 978–92–76-10386-8 (Online),978–92–76-10387-5 (Print).

Degraeuwe, B., Pisoni, E., Peduzzi, E., De Meij, A., Monforti-Ferrario, F., Bodis, K., Mascherpa, A., Astorga-Llorens, M., Thunis, P., Vignati, E., 2019b. Urban NO2 Atlas, Policy Assessment KJ-NA-29943-EN-N (Online), KJNA-29943-EN-C (Print), Luxembourg (Luxembourg).

Departament d'Avaluació i Gestió Ambiental, 2022. Zona de Baixes Emissions Rondes de Barcelona — Informe d'Implantació i Seguiment. https://ajuntament.barcelona.cat/premsa/wp-content/uploads/2022/03/Informe-implantacio-ZBE-VFFFdef.pdf.

Dun, M., Xu, Z., Chen, Y., Wu, L., 2020. Short-term air quality prediction based on fractional grey linear regression and support vector machine. Math. Probl. Eng. 2020, 1–13.
Dutheil, F., Baker, J., Navel, V., 2020. COVID-19 as a factor influencing air pollution? Environ. Pollut. 263, 114466.
Eder, B., Yu, S., 2006. A performance evaluation of the 2004 release of Models-3 CMAQ. Atmos. Environ. 40, 4811–4824.
Support vector regression methodology for wind turbine reaction torque prediction with power-split hydrostatic continuous variable transmission. Energy 67, 2014, 623–630.
European Environment Agency, 2021. National Emissions Reported to the Convention on Long-range Transboundary Air Pollution (LRTAP Convention), Data on Emissions of Air Pollutants Submitted to the LRTAP Convention and Copied to EEA. URL. https://www.eea.europa.eu/data-and-maps/daviz/contribution-of-the-transport-sector-6/download.table.
Fabregat, A., Vazquez, L., Vernet, A., 2021. Using machine learning to estimate the impact of ports and cruise ship traffic on urban air quality: the case of Barcelona. Environ. Model. Softw. 139, 104995.
Garcia Nieto, P.J., Combarro, E., Dıaz, J.J., Montanes, E., 2013. A SVM- based regression model to study the air quality at local scale in Oviedo urban area (Northern Spain): a case study. Appl. Math. Comput. 219, 8923–8937.
Gifford, F.A., 1976. Turbulent diffusion-typing schemes: a review. Nucl. Saf. 17 (1).
Gómez, N. Molina, Diaz-Arevalo, J., López-Jimenez, P., 2020. Air quality and urban sustainable development: the application of machine learning tools. Int. J. Environ. Sci. Technol. 18, 08.
Guevara, M., Martınez, F., Arevalo, G., Gass'o, S., Baldasano, J., 2013. An improved system for modelling Spanish emissions: HERMESv2.0. Atmos. Environ. 81, 209–221.
Guevara, M., Tena, C., Porquet, M., Jorba, O., C., 2019. Pérez Garćıa-Pando, HERMESv3, a stand-alone multi-scale atmospheric emission modelling framework – part 1: global and regional module. Geosci. Model Dev. 12 (5), 1885–1907.
Grup d'Avaluació de l'Impacte de la Zona de Baixes Emissions (ZBE) Rondes Barcelona, 2021. Avaluació de l'impacte de la ZBE en la qualitat de l'aire. https://www.aspb.cat/wp-content/uploads/2021/06/rondes-barcelona-qualitat-aire-2020.pdf.
Guevara, M., Jorba, O., Soret, A., Petetin, H., Bowdalo, D., Serradell, K., Tena, C., Denier van der Gon, H., Kuenen, J., Peuch, V.-H., Garc'ıa-Pando, C. Perez, 2021. Time-resolved emission reductions for atmospheric chemistry modelling in Europe during the COVID-19 lockdowns. Atmos. Chem. Phys. 21 (2), 773–797.
Kerimray, A., Baimatova, N., Ibragimova, O.P., Bukenov, B., Kenessov, B., Plotitsyn, P., Karaca, F., 2020. Assessing air quality changes in large cities during COVID-19 lockdowns: the impacts of traffic-free urban conditions in Almaty, Kazakhstan. Sci. Total Environ. 730, 139179.
Khomenko, S., Cirach, M., Pereira-Barboza, E., Mueller, N., Barrera-Gomez, J., Rojas-Rueda, D., Hoogh, K.D., Hoek, G., Nieuwenhuijsen, M., 2021. Premature mortality due to air pollution in European cities: a health impact assessment. Lancet Planet Health 5, 01.
Kleine Deters, J., Zalakeviciute, R., Gonzalez, M., Rybarczyk, Y., 2017. Modeling PM2.5 urban pollution using machine learning and selected meteorological parameters. J. Electric Comput. Eng. 1–14.
Kumar, K., Pande, D.B., 2022. Air pollution prediction with machine learning: a case study of Indian cities. Int. J. Environ. Sci. Technol. https://doi.org/10.1007/s13762-022-04241-5, 05.
Lateb, M., Meroney, R., Yataghene, M., Fellouah, H., Saleh, F., Boufadel, M., 2016. On the use of numerical modelling for near-field pollutant dispersion in urban environments — a review. Environ. Pollut. 208, 271–283.
Li, Z., Kovachki, N.B., Azizzadenesheli, K., Liu, B., Bhattacharya, K., Stuart, A.M., Anandkumar, A., 2020a. Fourier Neural Operator for Paramet- ric Partial Differential Equations. CoRR abs/2010.08895. arXiv: 2010.08895. URL. https://arxiv.org/abs/2010.08895.
Li, L., Li, Q., Huang, L., Wang, Q., Zhu, A., Xu, J., Liu, Z., Li, H., Shi, L., Li, R., Azari, M., Wang, Y., Zhang, X., Liu, Z., Zhu, Y., Zhang, K., Xue, S., Ooi, M.C.G., Zhang, D., Chan, A., 2020b. Air quality changes during the COVID-19 lockdown over the Yangtze River Delta Region: an insight into the impact of human activity pattern changes on air pollution variation. Sci. Total Environ. 732, 139282.
Li, Z., Ming, T., Liu, S., Peng, C., de Richter, R., Li, W., Zhang, H., Wen, C.-Y., 2021. Review on pollutant dispersion in urban areas-part a: effects of mechanical factors and urban morphology. Build. Environ. 190, 107534.
Liang, L., Gong, P., 2020. Urban and air pollution: a multi-city study of longterm effects of urban landscape patterns on air quality trends. Sci. Rep. 10, 18618.
Liu, B.C., Binaykia, A., Chang, P.-C., Tiwari, M., Tsao, C.-C., 2017. Urban air quality forecasting based on multi-dimensional collaborative Support Vector Regression (SVR): a case study of Beijing-Tianjin-Shijiazhuang. PLoS One 12, 07.
Lovric, M., Pavlovic, K., Vukovic, M., Grange, S.K., Haberl, M., Kern, R., 2021. Understanding the true effects of the COVID-19 lockdown on air pollution by means of machine learning. Environ. Pollut. 274, 115900.
Lu, W.-Z., Wang, W.-J., 2005. Potential assessment of the "support vector machine" method in forecasting ambient air pollutant trends. Chemosphere 59, 693–701.
Lu, L., Jin, P., Pang, G., Zhang, Z., Karniadakis, G.E., 2021. Learning nonlinear operators via deeponet based on the universal approximation theorem of operators. Nat. Mach. Intell. 3 (3), 218–229.
Ma, J., Cheng, J., Lin, C., Tan, Y., Zhang, J., 2019. Improving air quality prediction accuracy at larger temporal resolutions using deep learning and transfer learning techniques. Atmos. Environ. 214, 116885.
Masih, A., 2019. Machine Learning algorithms in air quality modeling. Glob. J. Environ. Sci. Manag. 5, 09.
Maynard, R., 2009. Health effects of urban pollution, issues in environmental. Sci. Technol. 28, 108–128.
Medi ambient i sostenibilitat, 2022. Generalitat de Catalunya (Environment and sustainability, Generalitat de Catalunya). http://mediambient.gencat.cat/ca/05ambits dactuacio/atmosfera/ qualitat de laire/vols-saber-que-respires/descarrega-de- dades/, Xarxa de Vigilància i Previsío de la Contaminaci'o Atmosèrica (Atmospheric Pollution Monitoring and Forecasting Network).
Munir, S., Mayfield, M., Coca, D., Mihaylova, L., Osammor, O., 2020. Analysis of air pollution in urban areas with Airviro dispersion model—a case study in the City of Sheffield, United Kingdom. Atmosphere 11, 285.
Nicolas, B., 2022. Personal Communication, The European Organisation for the Safety of Air Navigation (Eurocontrol) — Air Traffic Flow Management data and Statistics.
Open Data BCN, 2022a. https://opendata-ajuntament.barcelona.cat. Ajuntament de Barcelona (Barcelona City Hall).
Open Data BCN, 2022b. https://opendata-ajuntament.barcelona.cat/data/en/dataset/aforaments-descriptiu. Ajuntament de Barcelona (Barcelona City Hall).
Pasquill, F., 1976. Atmospheric Dispersion Parameters in Gaussian Plume Modeling; Part 2, Possible Requirements for Change in the Turner Workbook valuesEPA-600/4–76-030b.
Polezer, G., Tadano, Y., Siqueira, H., Godoi, A., Yamamoto, C., Andre, P., Pauliquevis, T., Andrade, M., Oliveira, A., Saldiva, P., Taylor, P., Godoi, R.H.M., 2018. Assessing the impact of PM2.5 on respiratory disease using artificial neural networks. Environ. Pollut. 235, 394–403.
Port of Barcelona Open Data Portal, 2022. https://opendata.portdebarcelona.cat. Port of Barcelona Open Data Portal.
Powers, J.G., Klemp, J.B., Skamarock, W.C., Davis, C.A., Dudhia, J., Gill, D.O., Coen, J.L., Gochis, D.J., Ahmadov, R., Peckham, S.E., Grell, G.A., Michalakes, J., Trahan, S., Benjamin, S.G., Alexander, C.R., Dimego, G.J., Wang, W., Schwartz, C.S., Romine, G.S., Liu, Z., Snyder, C., Chen, F., Barlage, M.J., Yu, W., Duda, M.G., 2017. The weather research and forecasting model: overview, system efforts, and future directions. Bull. Am. Meteorol. Soc. 98 (8), 1717–1737.
Rodriguez-Rey, D., Guevara, M., Linares, M.P., Casanovas, J., Armengol, J.M., Benavides, J., Soret, A., Jorba, O., Tena, C., Garc'ıa-Pando, C.P., 2022. To what extent the traffic restriction policies applied in Barcelona city can improve its air quality? Sci. Total Environ. 807, 150743.
Russo, A., Raischel, F., Lind, P., 2013. Air quality prediction using optimal neural networks with stochastic variables. Atmos. Environ. 79, 822–830.
Rybarczyk, Y., Zalakeviciute, R., 2021. Assessing the COVID-19 impact on air quality: a machine learning approach. Geophys. Res. Lett. 48 (4) e2020GL091202.
Sachdeva, S., Baksi, S., 2018. Air Pollutant Dispersion Models: A Review, pp. 203–207.
Servei Meteorològic de Catalunya (Catalan Meteorologic Service), 2022. Xarxa d'Estacions Meteorològiques Automàtiques (Network of Automatic Weather Stations). https://www.meteo.cat/wpweb/serveis/cataleg-de-serveis/dades-meteorologiques/.
Shamshirband, S., Petkovic, D., Javidnia, H., Gani, A., 2015. Sensor data fusion by support vector regression methodology — a comparative study. IEEE Sensors J. 15 (2), 850–854.

Simic, I., Lovric, M., Godec, R., Kroll, M., Beslic, I., 2020. Applying machine learning methods to better understand, model and estimate mass concentrations of traffic-related pollutants at a typical street canyon. J. Environ. Pollut. 263, 114587.
Singh, K., Gupta, S., Rai, P., 2013. Identifying pollution sources and predicting urban air quality using ensemble learning methods. Atmos. Environ. 80, 426–437.
Skamarock, W., Klemp, J., 2006. A time-split nonhydrostatic atmospheric model for research and NWP applications. J. Comput. Phys. 135, 08.
Sklearn package-SVR, 2022. https://scikit-learn.org/stable/modules/generated/sklearn.svm.SVR.html. Suport Vector Regression implementation.
Snyder, M.G., Venkatram, A., Heist, D.K., Perry, S.G., Petersen, W.B., Isakov, V., 2013. RLINE: a line source dispersion model for near-surface releases. Atmos. Environ. 77, 748–756.
Song, J., Han, K., Stettler, M.E.J., 2021. Deep-maps: machine-learning-based mobile air pollution sensing. IEEE Internet Things J. 8 (9), 7649–7660.
Wei, P., Zhenzhou, L., Song, J., 2015. Variable importance analysis: a comprehensive review. Reliab. Eng. Syst. Saf. 142, 06.
World Health Organization, 2021. WHO Global Air Quality Guidelines: Particulate Matter (PM2.5 and PM10), Ozone, Nitrogen Dioxide, Sulfur Dioxide and Carbon Monoxide. World Health Organization.
Yang, W., Deng, M., Xu, F., Wang, H., 2018. Prediction of hourly PM2.5 using a space-time support vector regression model. Atmos. Environ. 181, 03.
Yu, S., Eder, B., Dennis, R., Chu, S.-H., Schwartz, S.E., 2006. New unbiased symmetric metrics for evaluation of air quality models. Atmos. Sci. Lett. 7 (1), 26–34.
Zalakeviciute, R., Bastidas, M., Buenano, A., Rybarczyk, Y., 2020. A traffic- based method to predict and map urban air quality. Appl. Sci. 10, 2035.
Zhao, B., Yu, L., Wang, C., Shuai, C., Zhu, J., Qu, S., Taiebat, M., Xu, M., 2021. Urban air pollution mapping using fleet vehicles as mobile monitors and machine learning. Environ. Sci. Technol. 55, 03.